



Article

Tracking Control of Physical Systems with Application to a System with a DC Motor: A Bond Graph Approach

Aaron Padilla Garcia ^{1,*} , Gilberto Gonzalez-Avalos ², Gerardo Ayala-Jaimes ³ , Noe Barrera Gallegos ⁴, Juancarlos Mendez-B. ² and David Alvarado-Zamora ²

¹ Faculty of Electrical Engineering, University of Michoacán, Morelia 58000, Mexico

² Graduate Studies Division, Faculty of Mechanical Engineering University of Michoacán, Morelia 58000, Mexico; gilberto.gonzalez@umich.mx (G.G.-A.); juancarlos.mendez@umich.mx (J.M.-B.); 0213483k@umich.mx (D.A.-Z.)

³ Faculty of Sciences of Engineering and Technology, Autonomous University of Baja California, Tijuana 22260, Mexico; ayala.gerardo@uabc.edu.mx

⁴ Faculty of Mechanical Engineering, University of Michoacán, Morelia 58000, Mexico; noe.barrera@umich.mx

* Correspondence: aaron.padilla@umich.mx

Abstract: In this paper, the bond graph modeling for the control of tracking systems has been applied. The closed loop system is built by the bond graph model of the system to be controlled, an additional bond graph according to the tracking input signal, and feedback gains in the physical domain. Hence, a procedure to obtain the closed loop tracking system is proposed. The proposal of modeling and tracking control systems in this paper determines symmetries in the bond graph approach with respect to the traditional algebraic approach. The great advantage of this graphical approach is that the mathematical determination of the system model is not necessary. Moreover, the coefficients of the characteristic polynomial using unidirectional causal loops of the closed loop system modeled in bond graphs are obtained. A case of study of a DC motor connected to an electrical supply network and a mechanical load is considered. Tracking control for the step, ramp, and acceleration type input signals in a bond graph approach are applied. In order to show the effectiveness of the proposed procedure, the simulation results are shown.

Keywords: bond graph; closed loop tracking system; controllability; causal paths; loops



Citation: Padilla Garcia, A.; Gonzalez-Avalos, G.; Ayala-Jaimes, G.; Barrera Gallegos, N.; Mendez-B., J.; Alvarado-Zamora, D. Tracking Control of Physical Systems with Application to a System with a DC Motor: A Bond Graph Approach. *Symmetry* **2022**, *14*, 755. <https://doi.org/10.3390/sym14040755>

Academic Editor: Christos Volos

Received: 5 March 2022

Accepted: 1 April 2022

Published: 6 April 2022

Publisher's Note: MDPI stays neutral with regard to jurisdictional claims in published maps and institutional affiliations.



Copyright: © 2022 by the authors. Licensee MDPI, Basel, Switzerland. This article is an open access article distributed under the terms and conditions of the Creative Commons Attribution (CC BY) license (<https://creativecommons.org/licenses/by/4.0/>).

1. Introduction

Many linear system control procedures have been applied to regulator design while system tracking controllers design has not received much attention. On the other hand, basic developments of tracking controllers have been published in [1–4]. Some references using different alternatives in tracking control systems and various applications can be found in [5–12].

Bond graph theory provides formal and unified procedures in the modeling of dynamic physical systems. Bond graphs determine state equations and transfer functions related to simulation results. The representation and exchange of the power of the elements that form a system is the main characteristic of bond graph modeling [13]. In addition, bond graphs allow modeling systems formed by different types of energy (electrical, mechanical, hydraulic, thermal), and their junction structure gives the structural properties of the systems [14].

The research question that can be mentioned is whether the bond graph methodology can be used in controller design, which is answered in this paper.

For a given input, the system inversion to get the input can be used. Hence, system inversion is an interesting methodology for control theory [15]. The construction of an inverse system for an LTI discrete system is considered in [16].

The mathematical models used in the classical inversion methods generally determine structural characteristics and physical interpretation that are difficult to interpret. In this way, bond graph models using the concept of bicausality give a correct direction to obtain inverse systems [17]. In [18], this concept is used to model the virtual earth, which allows simplifying the modeling electronic circuits with operational amplifiers. The control design in the development of complex supervision applying bond graphs with bicausality is proposed in [19].

In this paper, the design of tracking controllers applied to systems modeled in a bond graph is presented. The proposed procedure consists of the model of the system in the physical domain and an additional bond graph that determines the tracking controller. Likewise, this control is built by additional state variables for tracking the input signals and the feedback gains.

Currently, the research in bond graphs has been directed to the modeling of different physical systems with their applications, so this paper is a development in the design of tracking control systems in the physical domain. Likewise, due to the characteristics of bond graphs, this methodology can be applied to electrical, mechanical, hydraulic, and thermal systems. Furthermore, the system modeling, the controller design, and the determination of the feedback gains are obtained in the graphical approach only. These are the main motivations of this paper.

The tracking error of the proposal in this paper is zero. However, the control law to achieve this error requires that the system parameters be known and constant. Refs. [11,12] have solved this problem considering uncertain nonlinearities. Hence, future works correspond to consider models with unknown parameters and dynamics not modeled.

In order to obtain the closed-loop system, the conditions of controllability and observability have to be satisfied, which are determined in the physical domain.

Some of the main advantages of this paper with respect to previously published works follow. (1) The classical approach of tracking control [1,2,4–6,8,11,12,20] is based on an analysis of differential equations or state equations; if the system changes, it is not easy to adapt these modifications, while in bond graphs, the adaptation process is simple. (2) The papers mentioned are dedicated to specific models and the bond graph has a multi-domain energy characteristic. (3) Changing the command of the inputs implies simple changes in the closed-loop bond graph. (4) It is not necessary to determine the mathematical model of the system to find the closed-loop system. (5) The coefficients of the characteristic polynomial are obtained directly in symbolic form with causal loops in the physical domain. A basic proposal in the control of tracking systems in bond graph is described in [21]. However, in this paper, the control of systems modeled in bond graph with linearly-dependent state variables is given, and the ordered evolution of the controllers due to the type of tracking input is described in the DC motor case study.

An interesting approach in the characterization of the electromagnetic compatibility of DC motors considering the electromagnetic interferences that appear in the brushes and commutator is proposed in [22]. It may be interesting to apply a bond graph to electromagnetic compatibility in order to obtain some graphical characteristics.

In [23], the author proposed an intelligent planning model applied to unmanned aerial vehicles (UAVs) using mobile internet of things (MIoT), which can be thought of as a form of tracking control. In addition, a prediction method for traffic flow using neural networks is proposed in [24], which can be interpreted as a way to implement a tracking control. An adaptive tracking control with fractional-order PID applied to a DC motor is proposed in [25]. A robust switched control for the trajectory tracking of DC motors that is part of a mobil robot is introduced in [26].

Therefore, the main contribution of this paper is to present bond graph tools applied to system tracking control without requiring its mathematical model.

The modeling of systems in bond graphs represents a symmetry to the modeling in the state space of these systems. Likewise, in this paper, other symmetries are established:

the tracking control in the physical domain and the direct determination of the coefficients of the characteristic polynomial using causal loops in bond graphs.

The proposed methodology is applied to an electromechanical system as a case study. Based on the bond graph model of this system, the controllability and observability conditions to be satisfied are verified. Additional state variables to achieve tracking and feedback gains are connected to the model. In 20 Sim software (v1.4, Controllab Products, Netherlands), this complete system is simulated showing the effectiveness of the proposed methodology.

Section 2 summarizes the problem statement by describing the traditional tracking systems approach. The basic methodology of bond graphs is given in Section 3. The procedure for the design of the tracking control in systems modeled by bond graphs is presented in Section 4. The direct determination of the characteristic polynomial in a bond graph approach is described in Section 5. A case study applying the proposed procedure is developed in Section 6. Finally, Section 6 presents the conclusions.

2. Problem Statement

Consider a linear time-invariant system (LTI) described by

$$\begin{bmatrix} \dot{x}(t) \\ y(t) \end{bmatrix} = \begin{bmatrix} A & B \\ C & D \end{bmatrix} \begin{bmatrix} x(t) \\ u(t) \end{bmatrix} \quad (1)$$

where $x(t) \in \mathbb{R}^n$, $u(t) \in \mathbb{R}^p$, and $y(t) \in \mathbb{R}^q$ and for a polynomial input of the form [1,20]

$$r(t) = r_0 + r_1 t + r_2 t^2 + \dots + r_{\delta-1} t^{\delta-1} \quad (2)$$

then, the output vector $y(t)$ becomes equal to the input $r(t)$ under the steady-state conditions of

$$\lim_{t \rightarrow \infty} [r(t) - y(t)] = 0 \quad (3)$$

where $r(t) \in \mathbb{R}^q$ and the polynomial input has the property

$$\frac{d^\delta r(t)}{dt^\delta} = 0 \quad (4)$$

In summary, the system outputs track the system inputs according to (3) with the characteristic of the inputs given by (4). In the controller design, auxiliary state variables are required to consider the property (4), which is defined by

$$\begin{bmatrix} \dot{\lambda}_1(t) \\ \dot{\lambda}_2(t) \\ \vdots \\ \dot{\lambda}_\delta(t) \end{bmatrix} = \begin{bmatrix} 0 & 0 & \dots & 0 & 0 \\ 0 & 1 & \dots & 0 & 0 \\ \vdots & \vdots & \ddots & \vdots & \vdots \\ 0 & 0 & \dots & 1 & 0 \end{bmatrix} \begin{bmatrix} \lambda_1(t) \\ \lambda_2(t) \\ \vdots \\ \lambda_{\delta-1}(t) \\ \lambda_\delta(t) \end{bmatrix} + \begin{bmatrix} r(t) - y(t) \\ 0 \\ \vdots \\ 0 \end{bmatrix} \quad (5)$$

where $\lambda_1(t) \in \mathbb{R}^q$, $\lambda_2(t) \in \mathbb{R}^q$, \dots , $\lambda_{\delta-1}(t) \in \mathbb{R}^q$ are the additional state variables due to integrators.

The open loop tracking system is built by the original model (1) and the additional state variables model (5), which is defined by

$$\dot{x}_\lambda(t) = A_{OL} x_\lambda(t) + B_{OL} u(t) + Q_{OL} v(t) \quad (6)$$

where

$$A_{OL} = \begin{bmatrix} A & 0_{n \times \delta(q)} & 0_{n \times q} \\ -C & 0_{q \times \delta(q)} & 0_{q \times q} \\ 0_{\delta(q) \times n} & I_{\delta(q) \times \delta(q)} & 0_{\delta(q) \times q} \end{bmatrix}; B_{OL} = \begin{bmatrix} B \\ 0 \\ 0 \end{bmatrix}; Q_{OL} = \begin{bmatrix} 0 \\ I_{q \times q} \\ 0 \end{bmatrix} \quad (7)$$

The next step is to determine if the open loop tracking system is controllable. The controllability condition is established in the following theorem.

Theorem 1 ([1,20]). *The open loop tracking system given by (6) is controllable if and only if the following conditions are satisfied.*

The controllability matrix $C_o = [B \ AB \ A^2B \ \dots \ A^{n+\delta q}B]$ is the full rank $n + \delta q$. From (6) and (7), this matrix is described by

$$C_o = \begin{bmatrix} B & AB & A^2B & \dots & A^{n+\delta q-1}B \\ 0 & -CB & -CAB & \dots & -CA^{n+\delta q-2}B \\ 0 & 0 & -CB & \dots & -CA^{n+\delta q-3}B \\ \vdots & \vdots & \vdots & \ddots & \vdots \\ 0 & 0 & 0 & \dots & -CA^{n+\delta q-\delta-1}B \end{bmatrix} \quad (8)$$

then

$$\text{rank } C_o = n + \delta q - 1 \quad (9)$$

Once the system has been verified to be controllable, the feedback of the system-state variables and additional state variables is applied. The complete feedback is defined by

$$u(t) = [K_x \ K_{\lambda 1} \ K_{\lambda 2} \ \dots \ K_{\lambda \delta}] \begin{bmatrix} x(t) \\ \lambda_1(t) \\ \lambda_2(t) \\ \vdots \\ \lambda_{\delta}(t) \end{bmatrix} \quad (10)$$

where K_x is an $p \times n$ matrix and K_i ($i = 1, 2, \dots, \delta$) are $p \times q$ matrices.

Applying the feedback (10) to the open loop system (7), we obtain

$$\dot{x}_{\lambda}(t) = A_{CL}x_{\lambda}(t) + B_{CL}v(t) \quad (11)$$

where

$$A_{OL} = \begin{bmatrix} A + BK_x & BK_{\lambda} & BK_{\lambda \delta} \\ -C & 0_{q \times \delta(q)} & 0_{q \times q} \\ 0_{\delta(q) \times n} & I_{\delta(q) \times \delta(q)} & 0_{\delta(q) \times q} \end{bmatrix}; \quad B_{CL} = \begin{bmatrix} 0 \\ I_{q \times q} \\ 0 \end{bmatrix} \quad (12)$$

with

$$K_{\lambda} = [K_{\lambda 1} \ K_{\lambda 2} \ \dots \ K_{\lambda(\delta-1)}] \quad (13)$$

The essential elements in bond graph modeling are described in the next section.

3. Modeling in Bond Graph

The main characteristic in bond graph modeling is the power transfer in the system, which is obtained by the product of generalized variables of effort $e(t)$ and flow $f(t)$. This transfer is carried out in bonds drawn by a simple line with direction and causality. In addition, the energy stored and dissipated can be determined. Therefore, bond graph models derive equations directly, and structural analysis can be obtained [27].

The representation of a bond is shown in Figure 1.

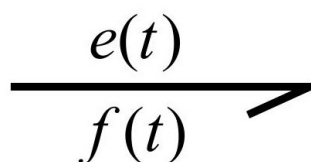


Figure 1. Power bond.

The power variables for some physical systems are indicated in Table 1.

Table 1. Power variables.

System	Effort ($e(t)$)	Flow ($f(t)$)
Mechanical	Force (F) Torque (τ)	Velocity (v) Ang. velocity (ω)
Electrical	Voltage (v)	Current (i)
Hydraulic	Pressure (P)	Volume flow rate (Q)

In addition, in this type of system modeling, it is necessary to know the energy variables denoted by momentum $p(t)$ and displacement $q(t)$ where $p(t) = \int e(t)dt$ and $q(t) = \int f(t)dt$. At each port, both an effort and a flow exist; if one of the effort or flow variables is an input, the other will be the output; this relationship is called causality. Hence, effort and flow are in opposite directions. A causal stroke represented by a short line perpendicular to the beginning or end of a bond allows causality to be assigned. In the direction of the causal stroke goes the direction of the effort $e(t)$, and in the opposite direction, the flow $f(t)$ will always be in a bond. A bond with the causal stroke is illustrated in Figure 2 [13,28].

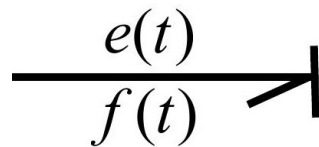


Figure 2. Causal bond.

Moreover, the sources, dissipation, and storage elements can be modeled in a bond graph, and Table 2 gives these elements with their causal relations.

Table 2. Causal forms for 1-ports.

Element	Causal Form	Causal Relation
Effort Source	$\text{MSe} \longrightarrow \dashv$	$e(t) = E(t)$
Flow Source	$\text{MSf} \dashv \longrightarrow$	$f(t) = F(t)$
Resistance	$\text{R} \longleftarrow \dashv$ $\text{R} \dashv \longrightarrow$	$e(t) = \Phi_R(f(t))$ $f(t) = \Phi_R^{-1}(e(t))$
Capacitance	$\text{C} \longleftarrow \dashv$ $\text{C} \dashv \longrightarrow$	$e(t) = \Phi_C(\int f(t)dt)$ $f(t) = \Phi_C^{-1}(\frac{de(t)}{dt})$
Inertia	$\text{C} \longleftarrow \dashv$ $\text{C} \dashv \longrightarrow$	$e(t) = \Phi_I(\int e(t)dt)$ $f(t) = \Phi_I^{-1}(\frac{df(t)}{dt})$

The block diagram of a Bond Graph in an Integral causality assignment (BGI) of an LTI system is shown in Figure 3 [14,28].

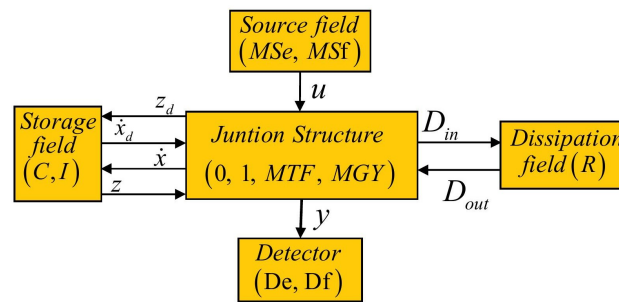


Figure 3. Key vectors of the BGI.

The elements of Figure 3 are as follows:

- (MS_e, MS_f) represent the effort and flow modulated sources.
- (C, I) denote the storage elements defined by capacitance and inertia, respectively.
- R represents the dissipation elements that constitute the resistors.
- $(0, 1, TF, GY)$ represent the junction structure with 0 and 1 junctions and the transformers and gyrators denoted by TF and GY , respectively.
- (D_e, D_f) determine the detectors for the effort and flow, respectively.

The energy variables are $p(t)$ and $q(t)$ related to elements I and C , respectively. The key vectors in Figure 3 are described by

- $x(t) \in \mathbb{R}^n$ and $x_d(t) \in \mathbb{R}^m$ represent the state variables for storage elements in integral and derivative causality assignments, respectively.
- $z(t) \in \mathbb{R}^n$ and $z_d(t) \in \mathbb{R}^m$ are the co-energy vectors for storage elements in integral and derivative causality assignments, respectively.
- $D_{in}(t) \in \mathbb{R}$ and $D_{out}(t) \in \mathbb{R}$ represent the relationships between the junction structure and dissipation elements.
- $u(t) \in \mathbb{R}^p$ and $y(t) \in \mathbb{R}^q$ determine the inputs and outputs of the system, respectively.

The relationships of the storage and dissipation fields are expressed by

$$z(t) = Fx(t) \quad (14)$$

$$z_d(t) = F_d x_d(t) \quad (15)$$

$$D_{out}(t) = LD_{in}(t) \quad (16)$$

The relationships of the junction structure are given by

$$\begin{bmatrix} \dot{x}(t) \\ D_{in}(t) \\ y(t) \\ z_d(t) \end{bmatrix} = \begin{bmatrix} S_{11} & S_{12} & S_{13} & S_{14} \\ S_{21} & S_{22} & S_{23} & 0 \\ S_{31} & S_{32} & S_{33} & 0 \\ S_{41} & 0 & 0 & 0 \end{bmatrix} \begin{bmatrix} z(t) \\ D_{out}(t) \\ u(t) \\ \dot{x}_d(t) \end{bmatrix} \quad (17)$$

The values of the matrix S are in the set of $\{0, \pm 1, \pm k_t, \pm k_g\}$ where k_t and k_g are transformer and gyrator modules. There are two important properties related to this matrix S :

- S_{11} and S_{22} are square skew-symmetric matrices.
- S_{12} and S_{21} are matrices in which each other negatively transpose.

The state-space equations of the bond graph model are defined by [14,28]

$$\dot{x}(t) = Ax(t) + Bu(t) \quad (18)$$

$$y(t) = Cx(t) + Du(t) \quad (19)$$

where

$$A = E^{-1}(S_{11} + S_{12}MS_{21})F \quad (20)$$

$$B = E^{-1}(S_{13} + S_{12}MS_{23}) \quad (21)$$

$$C = (S_{31} + S_{32}MS_{21})F \quad (22)$$

$$D = S_{33} + S_{32}MS_{23} \quad (23)$$

with

$$E = I - S_{14}F_d^{-1}S_{41}F \quad (24)$$

being

$$M = (I - LS_{22})^{-1}L \quad (25)$$

Graphical procedures to determine the structural controllability and observability are defined in the following properties.

Property 1 ([29]). A bond graph model is structurally controllable if the following two conditions are satisfied:

1. The storage elements (I, C) in the integral causality assignment are causally connected with some control source (MS_e, MS_f) in the bond graph with preferred integral causality.
2. All storage elements (I, C) in integral causality in the bond graph with preferred integral causality can change to a derivative causality assignment. If it is not satisfied directly, a dualization of some MS_e or MS_f sources has to be applied in order to change the remaining integral causalities.

Property 2 ([29]). A bond graph model is structurally observable if the following two conditions are satisfied:

1. The storage elements (I, C) in the integral causality assignment are causally connected with some sensor (D_e, D_f) in the bond graph with preferred integral causality.
2. All storage elements (I, C) in integral causality in the bond graph with preferred integral causality can change to a derivative causality assignment. If it is not satisfied directly, a dualization of some D_e or D_f sources has to be applied in order to change the remaining integral causalities.

The causal paths are defined in Appendix A.

A procedure to build the tracking control applied to a bond graph model is presented in the next section.

4. Design of a Tracking Controller in a Bond Graph Approach

The general scheme of the tracking control is illustrated in Figure 4 in which it is desired to control the plant described in state space (1). The controller is defined by a number δ of additional state variables to achieve the tracking of plant outputs $y(t)$ to inputs $r(t)$ given by (2). In order to achieve system stabilization, control law (10) through feedback gains is determined. This feedback is a function of the gains applied to the plant states $x(t)$ and to the additional states $\lambda(t)$ to supply to the plant input $u(t)$.

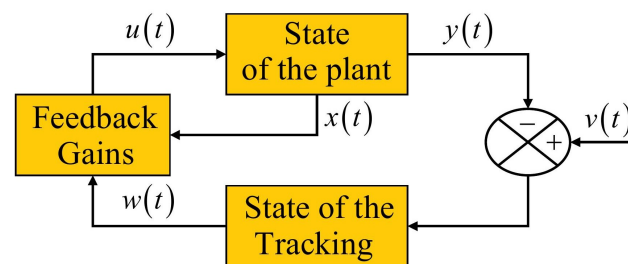


Figure 4. Scheme of the system with a tracking controller.

A first step in tracking control is the design of the open loop tracking system in the physical domain, which is shown in Figure 5. The scheme of the model in the bond graph of the plant is formed by the fields of sources, dissipation, and storage with the junction structure that determines the interconnection between its elements. The detector block allows to obtain the outputs for the plant. The desired tracking inputs r are connected through a new source field with a junction structure in order to connect the new storage field for additional state variables.

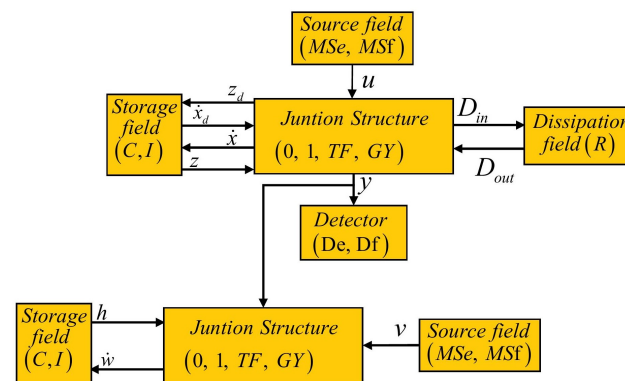


Figure 5. Open loop system using junction structure in bond graph models.

According to (6) with (7), the open loop tracking system requires r additional state variables, as illustrated in Figure 3. The additional states are defined by $\lambda(t)$, the energy vector is $\dot{\lambda}(t)$, the co-energy vector is $\sigma(t)$, and the desired inputs are $r(t)$.

From the block diagram of Figure 5, the junction structure for the open loop tracking system in a bond graph approach is presented by

$$\begin{bmatrix} \dot{x}(t) \\ D_{in}(t) \\ y(t) \\ z_d(t) \\ \hline \dot{\lambda}_1(t) \\ \dot{\lambda}_2(t) \\ \vdots \\ \dot{\lambda}_{\delta-1}(t) \\ \dot{\lambda}_{\delta}(t) \end{bmatrix} = \begin{bmatrix} S_{11} & S_{12} & S_{13} & S_{14} & 0 & 0 & 0 & \cdots & 0 & 0 \\ S_{21} & S_{22} & S_{23} & 0 & 0 & 0 & 0 & \cdots & 0 & 0 \\ S_{31} & S_{32} & 0 & 0 & 0 & 0 & 0 & \cdots & 0 & 0 \\ S_{41} & 0 & 0 & 0 & 0 & 0 & 0 & \cdots & 0 & 0 \\ \hline -S_{31} & -S_{32} & 0 & 0 & I & 0 & 0 & \cdots & 0 & 0 \\ 0 & 0 & 0 & 0 & 0 & I & 0 & \cdots & 0 & 0 \\ \vdots & \vdots & \vdots & \vdots & \vdots & \vdots & \vdots & \ddots & \vdots & \vdots \\ 0 & 0 & 0 & 0 & 0 & 0 & 0 & \cdots & 0 & 0 \\ 0 & 0 & 0 & 0 & 0 & 0 & 0 & \cdots & I & 0 \end{bmatrix} \begin{bmatrix} z(t) \\ D_{out}(t) \\ u(t) \\ \dot{x}_d(t) \\ \hline r(t) \\ \sigma_1(t) \\ \sigma_2(t) \\ \vdots \\ \sigma_{\delta-1}(t) \\ \sigma_{\delta}(t) \end{bmatrix} \quad (26)$$

the constitutive relationships for the new state variables are expressed by

$$\sigma_i(t) = F_i \lambda_i(t) \quad \forall i = 1, \dots, \delta \quad (27)$$

where F_i are constant and diagonal matrices and can be the identity matrices I .

It is interesting to note that the proposed junction structure is simple and only requires additional state variables of the order of the command input.

The last step to get the tracking control system in a bond graph approach is to introduce the control law given by (10) with Figure 2; then, a block diagram of the closed loop system is shown in Figure 6.

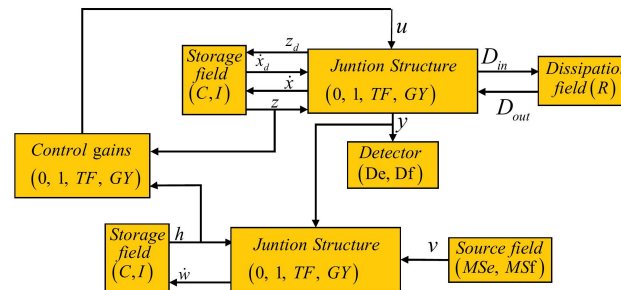


Figure 6. Closed loop system using junction structures.

A state feedback given by (10) is applied being the junction structure of this system defined by

$$\begin{bmatrix} \dot{x}(t) \\ D_{in}(t) \\ y(t) \\ z_d(t) \\ \dot{\lambda}_1(t) \\ \dot{\lambda}_2(t) \\ \vdots \\ \dot{\lambda}_{\delta-1}(t) \\ \dot{\lambda}_{\delta}(t) \end{bmatrix} = \begin{bmatrix} S_{11} + S_{13}K_g & S_{12} & S_{14} & 0 & K_{g1} & K_{g2} & \cdots & K_{g(r-1)} & K_{gr} \\ S_{21} + S_{23}K_g & S_{22} & 0 & 0 & 0 & 0 & \cdots & 0 & 0 \\ S_{31} & S_{32} & 0 & 0 & 0 & 0 & \cdots & 0 & 0 \\ S_{41} & 0 & 0 & 0 & 0 & 0 & \cdots & 0 & 0 \\ -S_{31} & -S_{32} & 0 & I & 0 & 0 & \cdots & 0 & 0 \\ 0 & 0 & 0 & 0 & I & 0 & \cdots & 0 & 0 \\ \vdots & \vdots & \vdots & \vdots & \vdots & \vdots & \ddots & \vdots & \vdots \\ 0 & 0 & 0 & 0 & 0 & 0 & \cdots & 0 & 0 \\ 0 & 0 & 0 & 0 & 0 & 0 & \cdots & I & 0 \end{bmatrix} \begin{bmatrix} z(t) \\ D_{out}(t) \\ \dot{x}_d(t) \\ v(t) \\ \sigma_1(t) \\ \sigma_2(t) \\ \vdots \\ \sigma_{\delta-1}(t) \\ \sigma_{\delta}(t) \end{bmatrix} \quad (28)$$

It can be shown that this approach for tracking systems consists of additional state variables and feedback gains of the complete state variables vector.

With the controller gains determined, the closed loop system is obtained. In a bond graph, these gains are implemented with TF and GY elements.

In order to obtain (28) with Figure 6, a graphical procedure for tracking systems in the physical domain is presented. The proposed procedure is the following:

Procedure 1.

1. Obtain a bond graph model in an integral causality assignment (BGI) of the system.
2. Verify the structural controllability and observability properties for the BGI.
3. Determine the index of (2) for command input.
4. Connect for each output the corresponding bond graph shown in Figure 7 for the additional state variables in order to get the open loop tracking system.

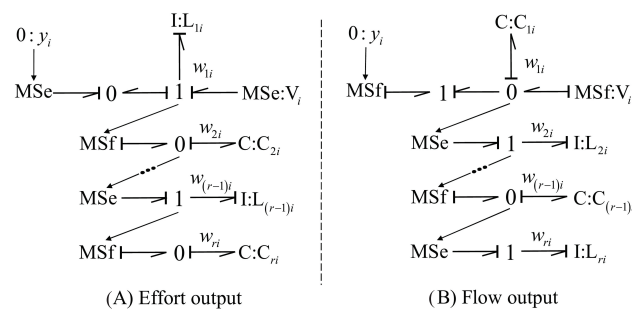


Figure 7. Bond graphs for the additional states.

5. The closed loop tracking system is obtained by calculating the feedback gains and connecting these gains according to Figure 8.

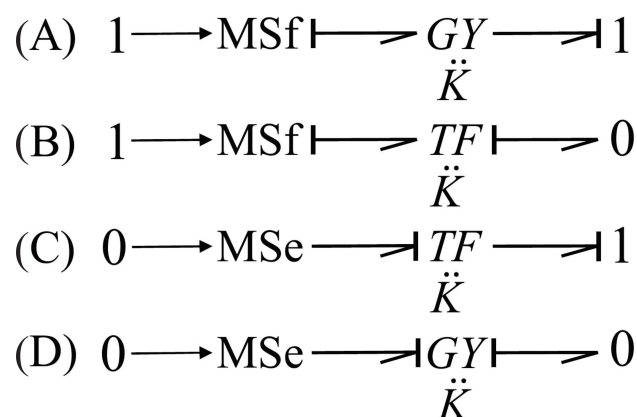


Figure 8. Feedback gains.

From the bond graph point of view, the proposed procedure consists of two stages:

1. The bond graph of the system to control which has to be controllable and observable according to properties 1 and 2.
2. The bond graph for the controller containing the number of additional state variables according to the tracking input (2) with Figure 7 and the feedback gains from Figure 8.

The interconnection between the bond graphs of the plant and the controller is obtained with bonds and 1 and 0 junctions determining the closed loop system in the physical domain.

For high-order systems, the bond graph approach can lead to difficulties due to the large number of bonds. However, by using submodels in 20Sim software, this problem can be reduced. With this paper, the modeling of systems of different energy domains and their tracking control can be solved in a single step. An interesting challenge for future work is to extend these results to a class of nonlinear systems.

5. Characteristic Polynomial of a Closed Loop System in the Physical Domain

The transfer function of an open loop system modeled by bond graphs using the loop rule is defined by [30],

$$\frac{Y(s)}{U(s)} = \frac{\sum_i T_i(s) \Delta_i(s)}{\Delta(s)} \quad (29)$$

with

$$\Delta(s) = 1 - \sum_i B_i + \sum_{i,j} B_i B_j - \sum_{i,j,k} B_i B_j B_k - \dots \quad (30)$$

where $T_i(s)$ is the forward path gain i ; $\sum_i B_i$ is the sum of all single causal loop gains; $\sum_{i,j} B_i B_j$ is the sum of products gain of all combinations of two nontouching single causal loops, $\sum_{i,j,k} B_i B_j B_k$ is the sum of gain products of all combinations of three nontouching single causal loops, and $\Delta_i(s)$ is similar to $\Delta(s)$ but excluding terms including single loops and their combinations that touch the i th forward path [30,31].

According to [32], the causal loops are obtained with power bonds following the flow and/or effort signal. However, in a closed loop system, the use of active bonds is required. Hence, in this paper, the determination of the characteristic polynomial of a closed loop system is presented.

In this case, the causal loops defined in (30) can now be unidirectional causal loops, which are loops that can have power bonds and active bonds, and this type of loop can

only exist in the direction of the active bonds that are required in the design of controllers in the bond graph approach.

Therefore, the model of the plant to be controlled, the tracking control, and the characteristic polynomial of the closed loop system are obtained in the physical domain.

The proposed methodology to obtain the closed loop tracking system in a bond graph approach is applied in the next section.

6. Case Study

The theory presented in previous sections can be conveniently illustrated by designing a controller that will cause the output of the controllable third-order linear plant whose Figure 9 shows a scheme of a DC motor connected to an RC network. However, in the mechanical load of the motor, a linearly dependent state variable is considered.

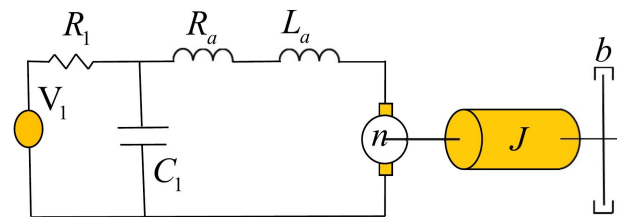


Figure 9. Scheme of a DC motor connected by an RC network.

Figure 9 describes the following elements: the supply voltage is V_1 , the resistance and the inductance of the armature winding are R_a and L_a , respectively; the inertia moment is J , the damping coefficient is b ; the electromechanical constant is n , and it is an R_1C_1 network. A mechanical connection with module a to consider a load moment of inertia J_e is applied.

The bond graph of this electromechanical system is shown in Figure 10.

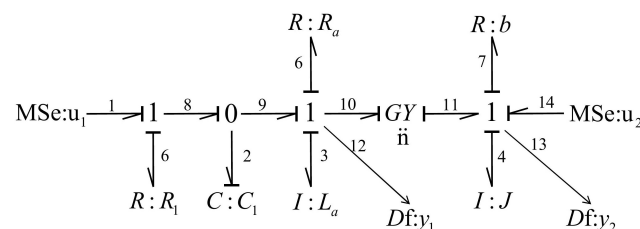


Figure 10. BGI of the system.

In this bond graph, the storage elements that are in an integral causality assignment are $(C : C_1, I : L_a, I : J)$ whose key vectors are expressed by

$$x = \begin{bmatrix} q_2 \\ p_3 \\ p_4 \end{bmatrix}; \dot{x} = \begin{bmatrix} f_2 \\ e_3 \\ e_4 \end{bmatrix}; z = \begin{bmatrix} e_2 \\ f_3 \\ f_4 \end{bmatrix}$$

with a constitutive relationship given by

$$F = \text{diag} \left\{ \frac{1}{C_1}, \frac{1}{L_a}, \frac{1}{J} \right\} \quad (31)$$

The storage element in a derivative causality assignment is $(I : J_e)$, which determines the linearly dependent state variable; the key vectors are

$$x_d = p_{17}; \dot{x}_d = e_{17}; z_d = f_{17}$$

and the constitutive relation

$$F_d = \frac{1}{J_e} \quad (32)$$

The key vectors for the dissipation elements are

$$D_{in} = \begin{bmatrix} e_5 \\ f_6 \\ f_7 \end{bmatrix}; D_{out} = \begin{bmatrix} f_5 \\ e_6 \\ e_7 \end{bmatrix}$$

where the constitutive relationship is

$$L = \text{diag} \left\{ \frac{1}{R_1}, R_a, b \right\} \quad (33)$$

This system has two inputs: the supply voltage ($MS_e : u_1$) and a load torque ($MS_e : u_2$), and two system outputs: ($D_f : y_1$) and ($D_f : y_2$), whose key vectors are

$$u = \begin{bmatrix} e_1 \\ e_{14} \end{bmatrix}; y = \begin{bmatrix} f_3 \\ f_4 \end{bmatrix}$$

The junction structure of the BGI is given by

$$\begin{bmatrix} f_2 \\ e_3 \\ e_4 \\ \hline e_5 \\ f_6 \\ f_7 \\ \hline f_3 \\ f_4 \\ \hline f_{17} \end{bmatrix} = \begin{bmatrix} 0 & -1 & 0 & 1 & 0 & 0 & 0 & 0 & 0 \\ 1 & 0 & -n & 0 & -1 & 0 & 0 & 0 & 0 \\ 0 & n & 0 & 0 & 0 & -1 & 0 & a & -a \\ \hline -1 & 0 & 0 & 0 & 0 & 0 & 1 & 0 & 0 \\ 0 & 1 & 0 & 0 & 0 & 0 & 0 & 0 & 0 \\ 0 & 0 & 1 & 0 & 0 & 0 & 0 & 0 & 0 \\ \hline 0 & 1 & 0 & 0 & 0 & 0 & 0 & 0 & 0 \\ 0 & 0 & 1 & 0 & 0 & 0 & 0 & 0 & 0 \\ \hline 0 & 0 & a & 0 & 0 & 0 & 0 & 0 & 0 \end{bmatrix} \begin{bmatrix} e_2 \\ f_3 \\ f_4 \\ \hline f_5 \\ e_6 \\ e_7 \\ \hline e_1 \\ e_{14} \\ \hline e_{17} \end{bmatrix} \quad (34)$$

Before building a system controller, it is necessary to verify the controllability and observability conditions. The causal paths for the two-control input u_1 are described by

- $MS_e : u_1 \mapsto C : C_1$ the causal path is (1 – 5 – 5 – 8 – 2).
- $MS_e : u_1 \mapsto I : L_a$ the causal path is (1 – 5 – 5 – 8 – 2 – 2 – 9 – 3).
- $MS_e : u_1 \mapsto I : J$ the causal path is (1 – 5 – 5 – 8 – 2 – 2 – 9 – 3 – 3 – 10 – 11 – 4).

and these causal paths are shown in Figure 11.

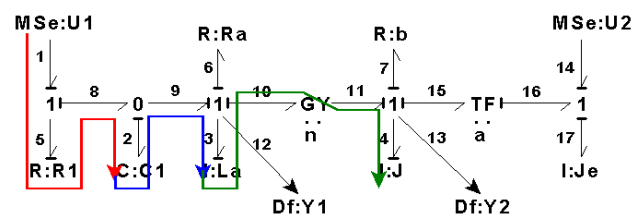


Figure 11. Causal paths from source $MS_e : u_1$ to storage elements.

Figure 12 shows the causal paths for the control input u_2 given by

- $MS_e : u_2 \mapsto I : J$ the causal path is (14 – 16 – 15 – 4).
- $MS_e : u_2 \mapsto I : L_a$ the causal path is (14 – 16 – 15 – 4 – 4 – 11 – 10 – 3).
- $MS_e : u_2 \mapsto C : C_1$ the causal path is (14 – 16 – 15 – 4 – 4 – 11 – 10 – 3 – 3 – 9 – 2).

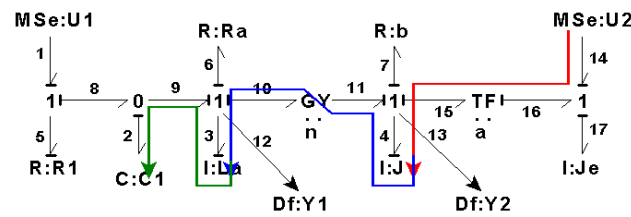


Figure 12. Causal paths from source $MSe : u_2$ to storage elements.

The causal paths from the storage elements (state variables) to the detectors (outputs) for y_1 are defined by

- $I : L_a \mapsto D_f : y_1$ the causal path is (3 – 12).
- $C : C_1 \mapsto D_f : y_1$ the causal path is (2 – 9 – 3 – 3 – 12).
- $I : J \mapsto D_f : y_1$ the causal path is (4 – 11 – 10 – 3 – 3 – 12).

and these causal paths are shown in Figure 13.

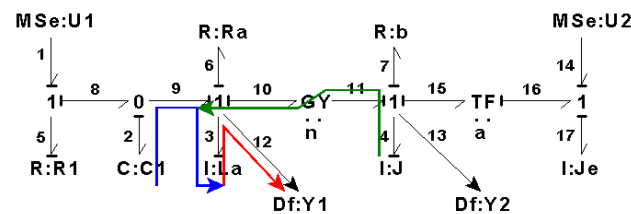


Figure 13. Causal paths from storage elements to detector $D_f : y_1$.

Figure 14 shows the causal paths for the output y_2 given by

- $I : J \mapsto D_f : y_2$ the causal path is (4 – 13).
- $I : L_a \mapsto D_f : y_2$ the causal path is (3 – 10 – 11 – 4 – 4 – 13).
- $C : C_1 \mapsto D_f : y_2$ the causal path is (2 – 9 – 3 – 3 – 10 – 11 – 4 – 4 – 13).

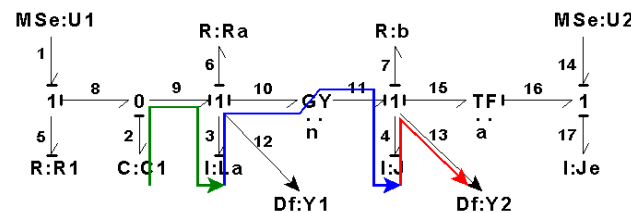


Figure 14. Causal paths from storage elements to detector $D_f : y_2$.

The corresponding bond graph in a derivative causality assignment (BGD) is shown in Figure 15.

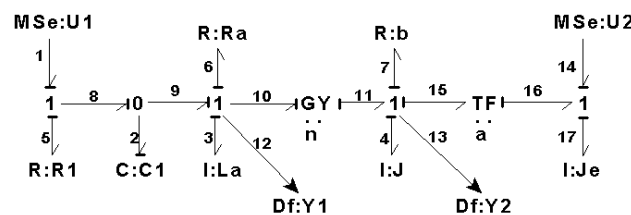


Figure 15. BGD of the system.

According to Properties 1 and 2, the system is structurally controllable and observable, and a tracking controller can be designed.

It is important to determine the coefficients of the characteristic polynomial for the design of the controller gains. The stabilization of the system and the convergence of the

outputs to the desired inputs is achieved by calculating the gains of the controller, which are obtained using the coefficients of the characteristic polynomial in closed loop. In a bond graph sense, these coefficients are obtained with the causal loops. Therefore, the characteristic polynomial for the bond graph model of Figure 10 is described by

$$S^3 + a_1 S^2 + a_2 S + a_3 = 0$$

- For a_1 , causal loops to a storage element are required.
 - $C : C_1 \leftrightarrow R : R_1$ the causal path is (2 – 8 – 5 – 5 – 8 – 2) denoted by

$$C_1 R_1(T) = \frac{1}{R_1 C_1} \quad (35)$$

- $I : L_a \leftrightarrow R : R_a$ the causal path is (3 – 6 – 6 – 3) with

$$L_a R_a(T) = \frac{R_a}{L_a} \quad (36)$$

- $I : J \leftrightarrow R : b$ the causal path is (4 – 7 – 7 – 4) with

$$J b(T) = \frac{b}{J} \quad (37)$$

and (4 – 15 – 16 – 17 – 17 – 16 – 15 – 14) with

$$J b_e(T) = \frac{J}{\Lambda} \quad (38)$$

where $\Lambda = J + a^2 J_e$ then

$$J b J_e(T) = J b(T) \cdot J b_e(T) = \frac{b}{J} \cdot \frac{J}{\Lambda} = \frac{b}{\Lambda} \quad (39)$$

this coefficient is defined by

$$a_1 = C_1 R_1(T) + L_a R_a(T) + J b J_e(T) = \frac{1}{R_1 C_1} + \frac{R_a}{L_a} + \frac{b}{\Lambda} \quad (40)$$

The causal loops are illustrated in Figure 16 where the red causal loop is (35), the blue causal loop is (36), and (39) is the green causal loop.

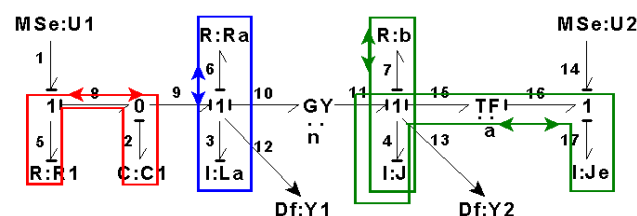


Figure 16. Causal loops for a_1 .

- For a_2 , causal loops containing two storage elements are required.
 - $C : C_1 \leftrightarrow I : L_a$ the causal path is (2 – 9 – 3 – 3 – 9 – 2) with

$$C_1 L_a(T) = \frac{1}{C_1 L_a} \quad (41)$$

- $(I : L_a \leftrightarrow I : J)$ the causal path is $(3 - 10 - 11 - 4 - 4 - 11 - 10 - 3)$

$$L_a J b J_e(T) = \frac{n^2}{L_a \Lambda} \quad (42)$$

- $(C : C_1 \leftrightarrow R : R_1)$ and $(I : L_a \leftrightarrow R : R_a)$ given by (35) and (36), respectively,

$$C_1 R_1(T) = C_1 R_1(T) \cdot L_a R_a(T) = \frac{1}{R_1 C_1} \cdot \frac{R_a}{L_a} = \frac{R_a}{R_1 C_1 L_a} \quad (43)$$

Figure 17 shows the causal loops for some terms of the coefficient a_2 where the red causal loop is (41), the blue causal loop is (42), and the green causal loop is (43).

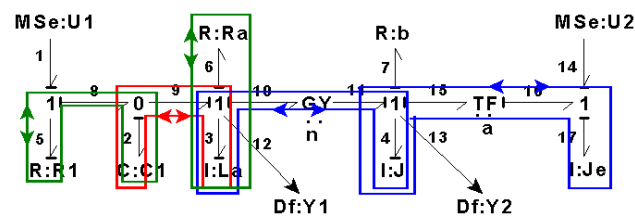


Figure 17. Causal loops for (44) and (45) of a_2 .

- – $(C : C_1 \leftrightarrow R : R_1)$ and $(I : J \leftrightarrow R : b)$ given by (35) and (39), respectively,

$$C_1 R_1(T) = C_1 R_1(T) \cdot J b J_e(T) = \frac{1}{R_1 C_1} \cdot \frac{b}{\Lambda} = \frac{b}{R_1 C_1 \Lambda} \quad (44)$$

- $(I : L_a \leftrightarrow R : R_a)$ and $(I : J \leftrightarrow R : b)$ given by (36) and (39), respectively,

$$L_a R_a(T) = L_a R_a(T) \cdot J b J_e(T) = \frac{R_a}{L_a} \cdot \frac{b}{\Lambda} = \frac{b R_a}{L_a \Lambda} \quad (45)$$

The rest of the terms for a_2 are illustrated in Figure 18 where the red causal loops is (44) and the blue causal loops is (45).

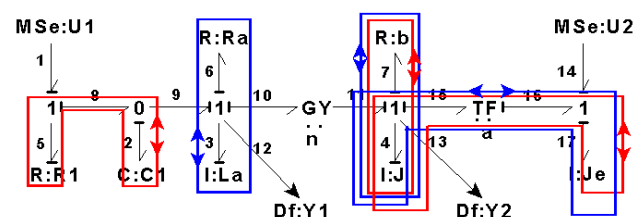


Figure 18. Causal loops for (44) and (45) of a_2 .

- This coefficient is described by

$$\begin{aligned} a_2 &= C_1 L_a(T) + L_a J b J_e(T) + \frac{C_1 R_1}{L_a R_a}(T) + \frac{C_1 R_1}{J b J_e}(T) + \frac{L_a R_a}{J b J_e}(T) \\ a_2 &= \frac{1}{C_1 L_a} + \frac{n^2}{L_a \Lambda} + \frac{R_a}{R_1 C_1 L_a} + \frac{b}{R_1 C_1 \Lambda} + \frac{b R_a}{L_a \Lambda} \end{aligned} \quad (46)$$

- For a_3 , causal loops are formed by three storage elements.

- $(C : C_1 \leftrightarrow I : L_a)$ and $(I : J \leftrightarrow R : b)$ given by (43), and (39), respectively,

$$C_1 L_a(T) = C_1 L_a(T) \cdot J b J_e(T) = \frac{1}{C_1 L_a} \cdot \frac{b}{\Lambda} = \frac{b}{C_1 L_a \Lambda} \quad (47)$$

- $(C : C_1 \leftrightarrow R : R_1)$, $(I : L_a \leftrightarrow R : R_a)$ and $(I : J \leftrightarrow R : b)$ given by (35), (36) and (39), respectively,

$$C_1 R_1 (T) \overset{JbJe}{L_a R_a} = C_1 R_1 (T) \cdot L_a R_a (T) \cdot JbJe (T) = \frac{1}{R_1 C_1} \cdot \frac{R_a}{L_a} \cdot \frac{b}{\Lambda} = \frac{b R_a}{R_1 C_1 L_a \Lambda} \quad (48)$$

- $(C : C_1 \leftrightarrow R : R_1)$, $(I : L_a \leftrightarrow R : R_a)$ and $(I : J \leftrightarrow R : b)$ given by (35) and (42), respectively,

$$C_1 R_1 (T) \overset{JbJe}{L_a} = \frac{1}{R_1 C_1} \cdot \frac{n^2}{L_a \Lambda} = \frac{n^2}{R_1 C_1 L_a \Lambda} \quad (49)$$

The causal loops for a_3 are shown in Figure 19 where (47) are the red causal loops, (48) are the blue causal loops, and (49) are the green causal loops.

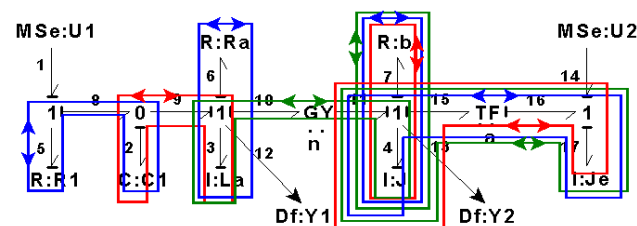


Figure 19. Causal loops for a_3 .

- This coefficient is

$$\begin{aligned} a_3 &= \overset{C_1 L_a}{JbJe} (T) + \overset{C_1 R_1}{L_a R_a} (T) \overset{JbJe}{L_a} + \overset{C_1 R_1}{L_a JbJe} (T) \\ a_3 &= \frac{b}{C_1 L_a \Lambda} + \frac{b R_a}{R_1 C_1 L_a \Lambda} + \frac{n^2}{R_1 C_1 L_a \Lambda} \end{aligned} \quad (50)$$

These coefficients will be used to determine the controller gains that are described below.

6.1. Step Tracking Control

The first tracking control to design is with an input command vector for constant steps defined by

$$\begin{bmatrix} r_1(t) \\ r_2(t) \end{bmatrix} = \begin{bmatrix} r_{01} \\ r_{02} \end{bmatrix} \quad (51)$$

In this case, it can be seen that the command input is of the form (2) and (51) with $\delta = 1$ and applying Procedure 1; Figure 20 shows the open loop tracking system in the physical domain.

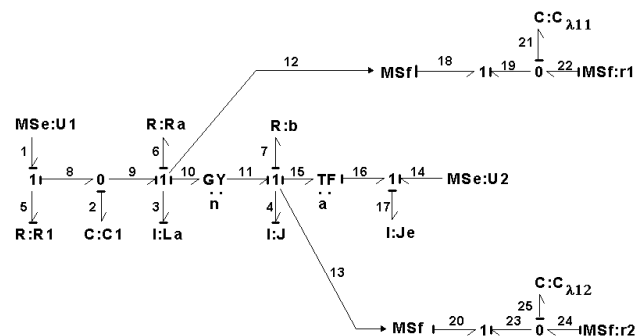


Figure 20. Open loop tracking system for steps.

The key vectors of the additional states for the bond graph of the open loop tracking system are defined by

$$\lambda_1 = \begin{bmatrix} q_{21} \\ q_{25} \end{bmatrix}; \dot{\lambda}_1 = \begin{bmatrix} f_{21} \\ f_{25} \end{bmatrix}; \sigma_1 = \begin{bmatrix} e_{21} \\ e_{25} \end{bmatrix}; r = \begin{bmatrix} f_{22} \\ f_{27} \end{bmatrix} \quad (52)$$

The junction structure of the open loop system is given by

$$\begin{bmatrix} f_2 \\ e_3 \\ e_4 \\ \hline e_5 \\ f_6 \\ f_7 \\ \hline f_3 \\ f_4 \\ \hline f_{17} \\ f_{21} \\ f_{25} \end{bmatrix} = \begin{bmatrix} 0 & -1 & 0 & 0 & 0 & 0 & 0 & 0 & 0 & 0 & 0 & 0 \\ 1 & 0 & -n & 0 & -1 & 0 & 0 & 0 & 0 & 0 & 0 & 0 \\ 0 & n & 0 & 0 & 0 & -1 & 0 & a & -a & 0 & 0 & 0 \\ \hline -1 & 0 & 0 & 0 & 0 & 0 & 1 & 0 & 0 & 0 & 0 & 0 \\ 0 & 1 & 0 & 0 & 0 & 0 & 0 & 0 & 0 & 0 & 0 & 0 \\ 0 & 0 & 1 & 0 & 0 & 0 & 0 & 0 & 0 & 0 & 0 & 0 \\ \hline 0 & 1 & 0 & 0 & 0 & 0 & 0 & 0 & 0 & 0 & 0 & 0 \\ 0 & 0 & 1 & 0 & 0 & 0 & 0 & 0 & 0 & 0 & 0 & 0 \\ \hline 0 & 0 & a & 0 & 0 & 0 & 0 & 0 & 1 & 0 & 0 & 0 \\ \hline 0 & -1 & 0 & 0 & 0 & 0 & 0 & 0 & 0 & 1 & 0 & 0 \\ 0 & 0 & -1 & 0 & 0 & 0 & 0 & 0 & 0 & 0 & 1 & 0 \end{bmatrix} \begin{bmatrix} e_2 \\ f_3 \\ f_4 \\ \hline f_5 \\ e_6 \\ e_7 \\ \hline e_1 \\ e_{14} \\ e_{17} \\ \hline f_{22} \\ f_{24} \\ \hline e_{21} \\ e_{25} \end{bmatrix} \quad (53)$$

Since the controllability condition is satisfied in this case, therefore, it is possible to synthesize a control law of the form (10) applied to these inputs in the following way

$$\begin{bmatrix} u_1 \\ u_2 \end{bmatrix} = \begin{bmatrix} (k_x)_{11} & (k_x)_{12} & (k_x)_{13} & (k_{\lambda 1})_{11} & (k_{\lambda 1})_{12} \\ 0 & 0 & 0 & (k_{\lambda 1})_{21} & 0 \end{bmatrix} \begin{bmatrix} q_2 \\ p_3 \\ p_4 \\ q_{21} \\ q_{26} \end{bmatrix} \quad (54)$$

Applying the controller gains from step 5 of Procedure 1, the bond graph of the closed loop tracking system is illustrated in Figure 21.

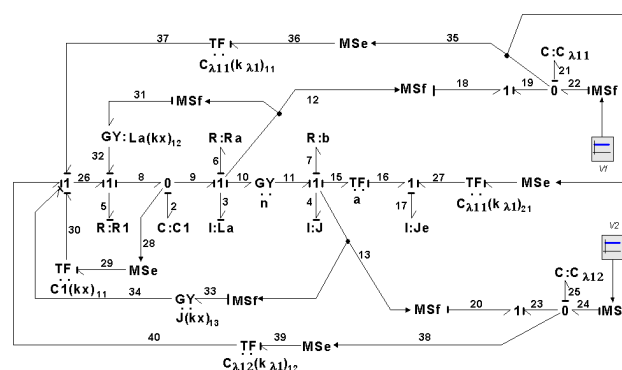


Figure 21. Closed loop tracking system for steps.

In order to obtain the gains for the controller, the characteristic polynomial of the closed loop system has to be determined. The order of the complete system is five, and the characteristic polynomial is given by

$$s^5 + b_1s^4 + b_2s^3 + b_3s^2 + b_4s + b_5 = 0 \quad (55)$$

The coefficients of this polynomial using causal paths are defined

- For b_1 : $(R : R_1 \longleftrightarrow C : C_1)$, $(R : R_a \longleftrightarrow I : L_a)$, $(R : b \longleftrightarrow I : J)$ given by (35), (36), and (39), respectively, and
 - $R : R_1 \longleftrightarrow C : C_1$ the causal path is $(2 - 28 - 29 - 30 - 26 - 5 - 5 - 8 - 2)$ shown in Figure 22 with

$$C_1(k_x)_{11}R_1(T) = \frac{-(k_x)_{11}}{R_1} \quad (56)$$

this causal loop is unidirectional due to the presence of feedback for the controller gain.

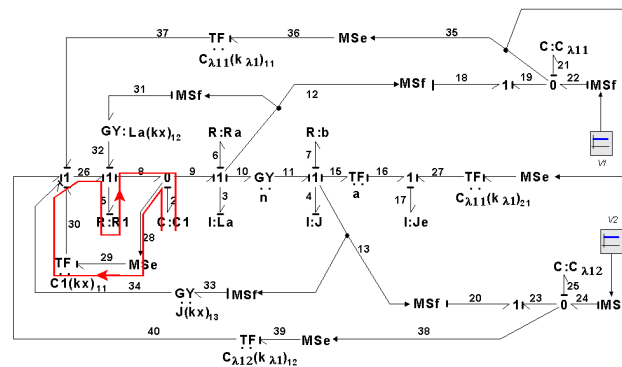


Figure 22. Unidirectional causal loop for (56).

Then

$$\begin{aligned} b_1 &= a_1 + C_1(k_x)_{11}R_1(T) \\ b_1 &= \frac{1}{R_1C_1} + \frac{R_a}{L_a} + \frac{b}{\Lambda} - \frac{(k_x)_{11}}{R_1} \end{aligned} \quad (57)$$

- For b_2 : $(C : C_1 \leftrightarrow I : L_a)$, $[(I : L_a \leftrightarrow R : R_a) \text{ and } (I : J \leftrightarrow R : b)]$, $[(C : C_1 \leftrightarrow R : R_1) \text{ and } (I : L_a \leftrightarrow R : R_a)]$, $[(C : C_1 \leftrightarrow R : R_1) \text{ and } (I : J \leftrightarrow R : b)]$, $[(I : L_a \leftrightarrow R : R_a) \text{ and } (I : J \leftrightarrow R : b)]$ defined by (41), (45), (44), (44) and (42), respectively, and
 - $(R : R_1 \longleftrightarrow C : C_1)$ and $(I : L_a \leftrightarrow R : R_a)$ given by (56) and (36), respectively

$$\frac{C_1(k_x)_{11}R_1(T)}{L_aR_a} = \frac{C_1(k_x)_{11}R_1(T)}{L_a} \cdot (T) = \frac{-(k_x)_{11}}{R_1} \cdot \frac{R_a}{L_a} \quad (58)$$

- $(R : R_1 \longleftrightarrow C : C_1)$ and $(I : J \leftrightarrow R : b)$ given by (56) and (39), respectively

$$\frac{C_1(k_x)_{11}R_1(T)}{JbJ_e} = \frac{C_1(k_x)_{11}R_1(T)}{JbJ_e} \cdot (T) = \frac{-(k_x)_{11}}{R_1} \cdot \frac{b}{\Lambda} \quad (59)$$

- $(I : L_a \leftrightarrow C : C_1)$ the causal path is $(3 - 12 - 31 - 32 - 5 - 5 - 8 - 2 - 2 - 9)$ with

$$L_a(k_x)_{12}C_1(T) = \frac{-(k_x)_{12}}{R_1C_1} \quad (60)$$

then

$$\begin{aligned} b_2 &= a_2 + \frac{C_1(k_x)_{11}R_1(T)}{L_aR_a} + \frac{C_1(k_x)_{11}R_1(T)}{JbJ_e} + L_a(k_x)_{12}C_1(T) \\ b_2 &= \frac{1}{C_1L_a} + \frac{n^2}{L_a\Lambda} + \frac{R_a}{R_1C_1L_a} + \frac{b}{R_1C_1\Lambda} + \frac{bR_a}{L_a\Lambda} \\ &\quad - \frac{(k_x)_{12}}{C_1R_1} - \frac{(k_x)_{11}R_a}{R_1L_a} - \frac{(k_x)_{11}b}{R_1\Lambda} \end{aligned} \quad (61)$$

Causal loops due to feedback gains are illustrated in Figure 23 where the red causal loop is (58), the blue causal loop is (59), and (60) is the green causal loop.

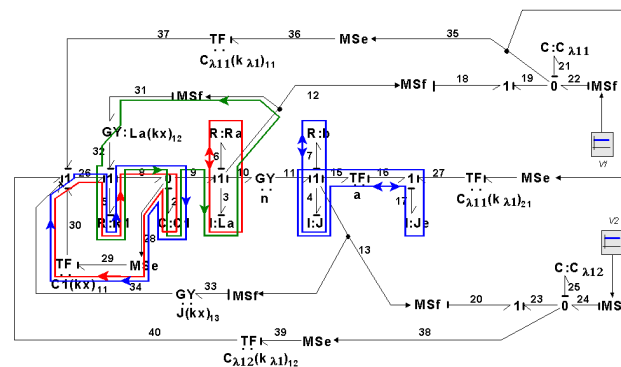


Figure 23. Unidirectional causal loop for (58), (59), and (60).

- For $b_3 : [(C : C_1 \leftrightarrow I : L_a) \text{ and } (I : J \leftrightarrow R : b)], [(C : C_1 \leftrightarrow R : R_1), (I : L_a \leftrightarrow R : R_a) \text{ and } (I : J \leftrightarrow R : b)], [(C : C_1 \leftrightarrow R : R_1), (I : L_a \leftrightarrow R : R_a) \text{ and } (I : J \leftrightarrow R : b)]$ defined by (47), (48), and (49), respectively, and
 - $(R : R_1 \longleftrightarrow C : C_1)$ and $[(I : L_a \leftrightarrow R : R_a) \text{ and } (I : J \leftrightarrow I : J_e)]$ given by (56) and (42), respectively,

$$\frac{C_1(k_x)_{11}R_1}{L_aJ}(T) = C_1(k_x)_{11}R_1(T) \cdot L_aJ(T) = \frac{-(k_x)_{11}}{R_1} \cdot \frac{n^2}{L_a\Lambda} \quad (62)$$

- $(R : R_1 \longleftrightarrow C : C_1)$, $[(I : L_a \leftrightarrow R : R_a) \text{ and } (I : J \leftrightarrow R : b)]$ given by (56), (36), and (39), respectively,

$$\frac{C_1(k_x)_{11}R_1}{L_aR_a}(T)JbJ_e = C_1(k_x)_{11}R_1(T) \cdot L_aR_a(T) \cdot JbJ_e(T) = \frac{-(k_x)_{11}}{R_1} \cdot \frac{R_a}{L_a} \cdot \frac{b}{\Lambda} \quad (63)$$

- $(I : L_a \longleftrightarrow C : C_1)$ and $(I : J \leftrightarrow R : b)$ given by (60) and (39), respectively,

$$\frac{L_a(k_x)_{12}C_1}{JbJ_e}(T) = L_a(k_x)_{12}C_1(T) \cdot JbJ_e(T) = \frac{-(k_x)_{12}}{R_1C_1} \cdot \frac{b}{\Lambda} \quad (64)$$

- $(I : J \longleftrightarrow I : J)$ the causal path is $(4 - 13 - 33 - 34 - 26 - 5 - 5 - 8 - 2 - 2 - 9 - 3 - 3 - 10 - 11)$ with

$$I(K_x)_{13}J(T) = \frac{-n(k_x)_{13}}{R_1C_1L_a} \cdot \frac{J}{\Lambda} \quad (65)$$

- $(C : C_{\lambda 11} \longleftrightarrow I : L_a)$ the causal path is $(21 - 35 - 36 - 37 - 26 - 5 - 5 - 8 - 2 - 2 - 9 - 3)$ with

$$C_{\lambda 11}(k_{\lambda})_{11}L_a(T) = \frac{-(k_{\lambda})_{11}}{R_1C_1L_a} \quad (66)$$

- $(C : C_{\lambda 11} \longleftrightarrow I : L_a)$ the causal path is $(21 - 35 - 41 - 27 - 16 - 15 - 4 - 4 - 11 - 10 - 3)$ with

$$C_{\lambda 11}(k_{\lambda})_{21}L_a(T) = \frac{-an(k_{\lambda})_{21}}{JL_a} \cdot \frac{J}{\Lambda} = \frac{-an(k_{\lambda})_{21}}{L_a\Lambda} \quad (67)$$

then

$$\begin{aligned}
 b_3 &= a_3 + \frac{C_1(k_x)_{11}R_1}{L_aJ}(T) + \frac{C_1(k_x)_{11}R_1}{L_aR_a}(T)JbJ_e + \frac{L_a(k_x)_{12}C_1}{JbJ_e}(T) + J(k_{\lambda 1})_{13}J(T) \\
 &\quad + C_{\lambda 11}(k_{\lambda 1})_{11}L_a(T) + C_{\lambda 11}(k_{\lambda 1})_{21}L_a(T) \\
 b_3 &= \frac{b}{C_1L_a\Lambda} + \frac{bR_a}{R_1C_1L_a\Lambda} + \frac{n^2}{R_1C_1L_a\Lambda} - \frac{(k_x)_{11}n^2}{R_1L_a\Lambda} - \frac{(k_x)_{11}R_ab}{R_1L_a\Lambda} - \frac{(k_x)_{12}b}{R_1C_1\Lambda} \\
 &\quad - \frac{n(k_x)_{13}J}{R_1C_1L_a\Lambda} + \frac{(k_{\lambda 1})_{11}}{R_1C_1L_a} - \frac{an(k_{\lambda 1})_{21}}{L_a\Lambda}
 \end{aligned} \quad (68)$$

Figure 24 shows the causal loops for the term (62) being the red causal loops and (63) being the blue causal loops.

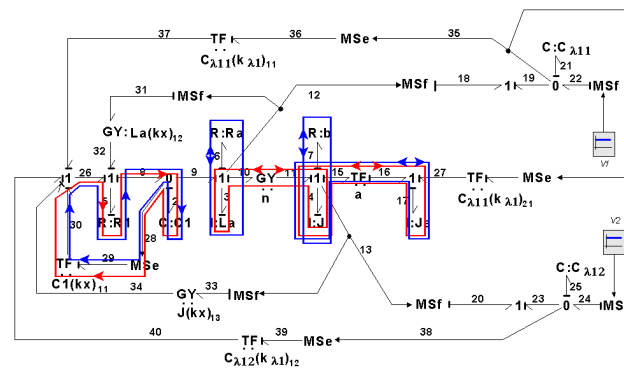


Figure 24. Causal loops for (62) and (63).

Figure 25 shows the red causal loops for (64) and (65) is the blue causal loop.

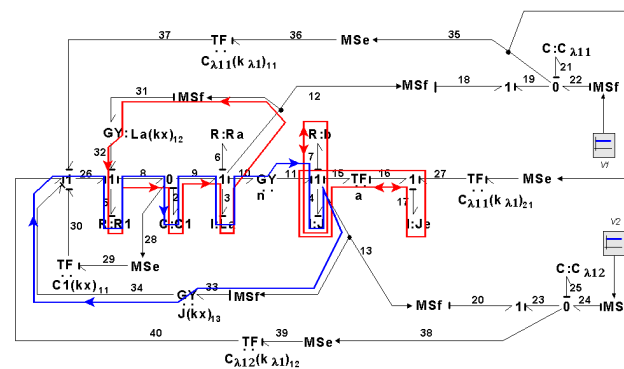


Figure 25. Causal loops for (64) and (65).

Figure 26 shows the red causal loops for (66) and (67) is the blue causal loop.

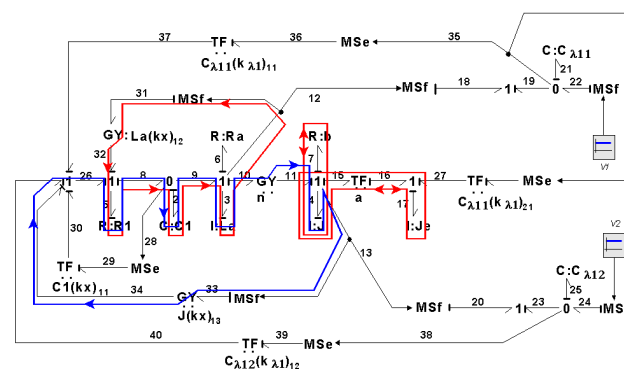


Figure 26. Causal loops for (66) and (67).

- For b_4
 - $(C : C_{\lambda 11} \longleftrightarrow I : L_a)$ and $(I : J \longleftrightarrow R : b)$ given by (66) and (39), respectively,

$$\frac{C_{\lambda 11}(k_{\lambda 1})_{11} L_a}{J b J_e}(T) = C_{\lambda 11}(k_{\lambda 1})_{11} L_a(T) \cdot J b J_e(T) = \frac{(k_{\lambda 1})_{11}}{R_1 C_1 L_a} \cdot \frac{b}{\Lambda} \quad (69)$$

and Figure 27 shows this causal loop.

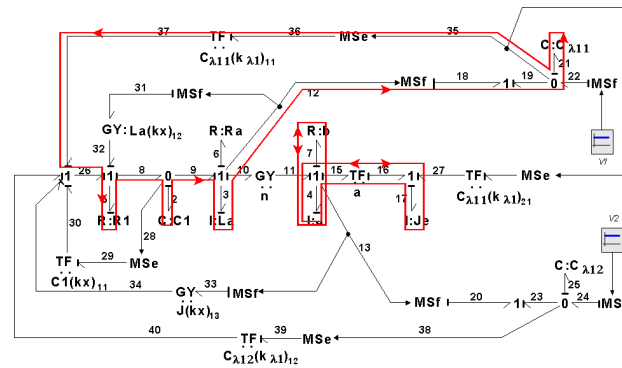


Figure 27. Causal loops for (69).

- – $(C : C_{\lambda 12} \longleftrightarrow C : C_{\lambda 12})$ the causal path is (25 – 38 – 39 – 40 – 26 – 5 – 5 – 8 – 9 – 3 – 3 – 10 – 11 – 4 – 4 – 13 – 20 – 23) with

$$\frac{C_{\lambda 12}(k_{\lambda 1})_{12} J}{J J_e}(T) = C_{\lambda 12}(k_{\lambda 1})_{12} J(T) \cdot J J_e(T) = \frac{n(k_{\lambda 1})_{12}}{R_1 C_1 L_a J} \cdot \frac{J}{\Lambda} \quad (70)$$

this term is shown in Figure 28.

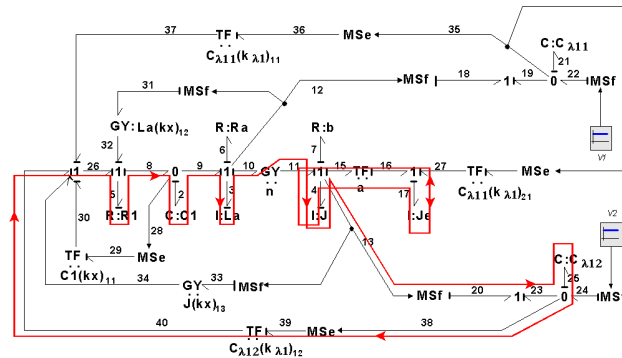


Figure 28. Causal loops for (70).

- – $(C : C_{\lambda 11} \longleftrightarrow C : C_{\lambda 11})$ and $(C : C_1 \longleftrightarrow R : R_1)$ given by (67) and (35), respectively,

$$\frac{C_{\lambda 11}(k_{\lambda 1})_{21} L_a}{C_1 R_1}(T) = C_{\lambda 11}(k_{\lambda 1})_{21} L_a(T) \cdot C_1 R_1(T) = \frac{-an(k_{\lambda 1})_{21}}{L_a \Lambda} \cdot \frac{1}{R_1 C_1} \quad (71)$$

this term is shown in Figure 29.

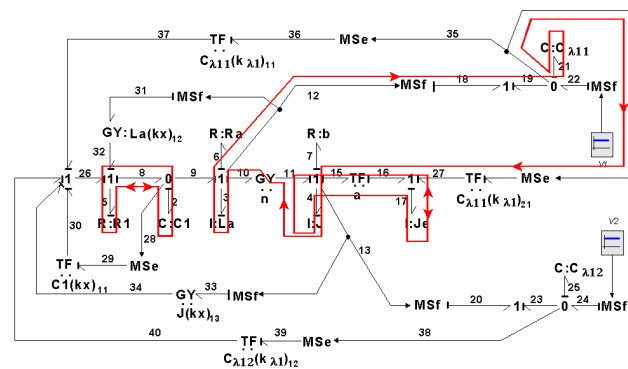


Figure 29. Causal loops for (71).

- $(C : C_{\lambda 11} \longleftrightarrow C : C_{\lambda 11})$ and $(C : C_1 \longleftrightarrow R : R_1)$ given by (67) and (56), respectively,

$$\frac{C_{\lambda 11}(k_{\lambda 1})_{21} L_a}{C_1 k_1 R_1}(T) = \frac{C_{\lambda 11}(k_{\lambda 1})_{21} L_a}{C_1 k_1 R_1}(T) \cdot C_1(k_{\lambda 1})_{11} R_1(T) = \frac{-an(k_{\lambda 1})_{21}}{L_a \Lambda} \cdot \frac{(k_x)_{11}}{R_1} \quad (72)$$

which is shown in Figure 30.

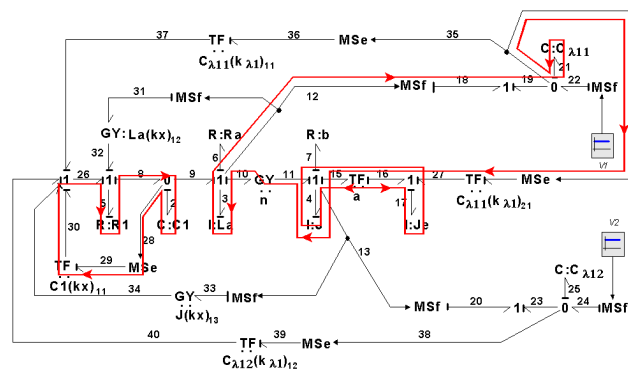


Figure 30. Causal loops for (72).

- $(C : C_{\lambda 11} \longleftrightarrow I : J)$ the causal path is (21 – 35 – 41 – 27 – 16 – 15 – 4 – 4 – 13 – 33 – 34 – 26 – 5 – 5 – 8 – 2 – 2 – 9 – 3) with

$$\frac{C_{\lambda 11}(k_{\lambda 1})_{21} L_a}{R_1 C_1 L_a \Lambda}(T) = \frac{J a(k_x)_{13}(k_{\lambda 1})_{21}}{R_1 C_1 L_a \Lambda} \quad (73)$$

shown in Figure 31.

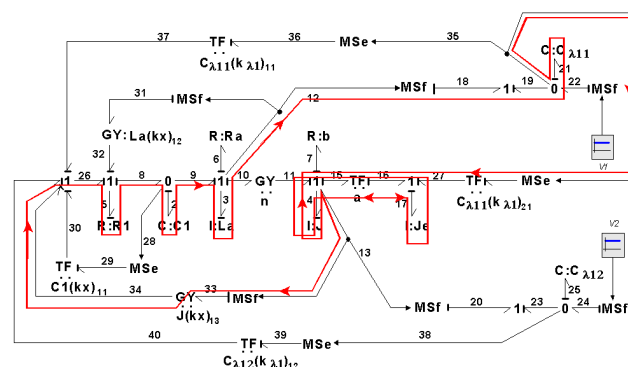


Figure 31. Causal loops for (73).

- – Then

$$\begin{aligned}
 b_4 &= a_4 + \frac{C_{\lambda 11}(k_{\lambda 1})_{11} L_a}{J b J_e}(T) + \frac{C_{\lambda 2}(k_{\lambda 1})_{12} J}{J J_e}(T) + \frac{C_{\lambda 11}(k_{\lambda 1})_{21} L_a}{C_1 R_1}(T) + \frac{C_{\lambda 11}(k_{\lambda 1})_{21} L_a}{C_1 (k_{\lambda 1})_{11} R_1}(T) \\
 &\quad + C_{\lambda 11}(k_{\lambda 1})_{21} L_a(T) \\
 b_4 &= \frac{n(k_{\lambda 1})_{12}}{R_1 C_1 L_a J} \cdot \frac{J}{\Lambda} + \frac{(k_{\lambda 1})_{11}}{R_1 C_1 L_a} \cdot \frac{b}{\Lambda} - \frac{a n(k_{\lambda 1})_{21}}{L_a \Lambda} \cdot \frac{1}{R_1 C_1} - \frac{a n(k_{\lambda 1})_{21}}{L_a \Lambda} \cdot \frac{(k_x)_1}{R_1 C_1} \\
 &\quad + \frac{J a (k_x)_3 (k_{\lambda 1})_{21}}{R_1 C_1 L_a \Lambda} \quad (74)
 \end{aligned}$$

- For b_5 , the only causal loop required is $(C : C_{\lambda 2} \longleftrightarrow C : C_{\lambda 2})$ with $(25 - 38 - 39 - 40 - 26 - 5 - 5 - 8 - 2 - 2 - 9 - 3 - 3 - 12 - 18 - 19 - 21 - 21 - 35 - 41 - 27 - 16 - 15 - 13 - 20 - 23)$ where

$$b_5 = \frac{-a(k_{\lambda 1})_{12}(k_{\lambda 1})_{21}}{R_1 C_1 L_a \Lambda} \quad (75)$$

and Figure 32 shows this term.

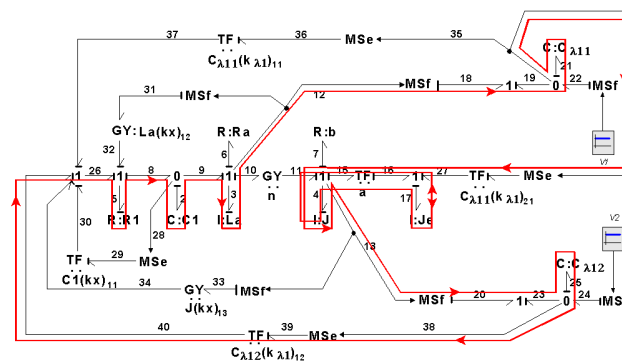


Figure 32. Causal loop for b_5 .

The numerical parameters used to carry out the simulation of the system are given in Table 3.

Table 3. Numerical parameters of the system.

$R_1 = 2 \Omega$	$L_a = 0.01 \text{ H}$	$b = 1.2 \text{ N-s/m}$	$n = 0.1$	$J_e = 0.625 \text{ N-m-s}^2$
$C_1 = 0.02 \text{ F}$	$R_a = 0.1 \Omega$	$J = 0.4 \text{ N-m-s}^2$	$a = 0.4$	

Then, the calculated controller gains so that the eigenvalues are all assigned the value -1 are shown in Table 4.

Table 4. Gains for the step tracking controller with eigenvalues at -1 .

$(k_x)_{11} = 64.8$	$(k_x)_{12} = 196.97$	$(k_x)_{13} = -0.05188$
$(k_{\lambda 1})_{11} = 0.00413$	$(k_{\lambda 1})_{12} = -0.04$	$(k_{\lambda 1})_{21} = 0.01$

The behavior of the system outputs are shown in Figure 33. The inputs at $t = 0$ are $V_1 = 5.2 \text{ A}$ and $V_2 = 1.25 \text{ rad/s}$; then, at $t = 30 \text{ s}$, there is an increment $\Delta V_1 = 0.8 \text{ A}$, and at $t = 60 \text{ s}$, the other input is increased by $\Delta V_2 = 0.8 \text{ rad/s}$. It is clear that the control performs its function effectively.

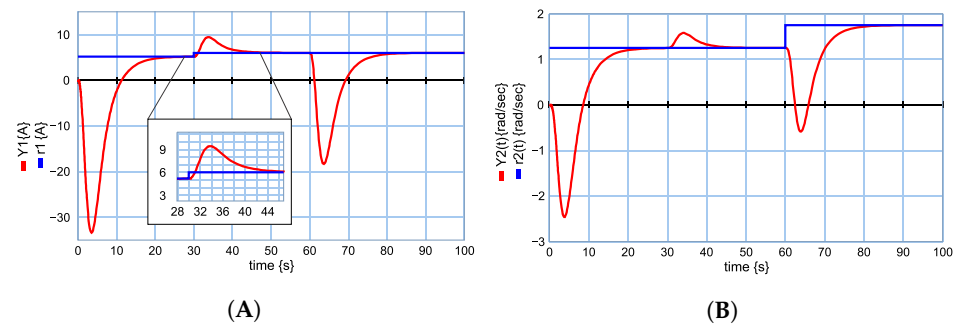


Figure 33. System outputs with a step tracking control with all eigenvalues at -1 : (A) Input r_1 and output y_1 ; (B) Input r_2 and output y_2 .

In order to stabilize the outputs of the system with smaller transients, all the eigenvalues are assigned in -10 , and the new gains are given in Table 5.

Table 5. Gains for the step tracking controller with eigenvalues at -10 .

$(k_x)_{11} = -25.2$	$(k_x)_{12} = 179.69$	$(k_x)_{13} = 3.5106$
$(k_{\lambda 1})_{11} = 3.4424$	$(k_{\lambda 1})_{12} = -4$	$(k_{\lambda 1})_{21} = 10$

The conditions of the inputs are the same as those described above, and Figure 34 illustrates the dynamic behavior of the outputs.

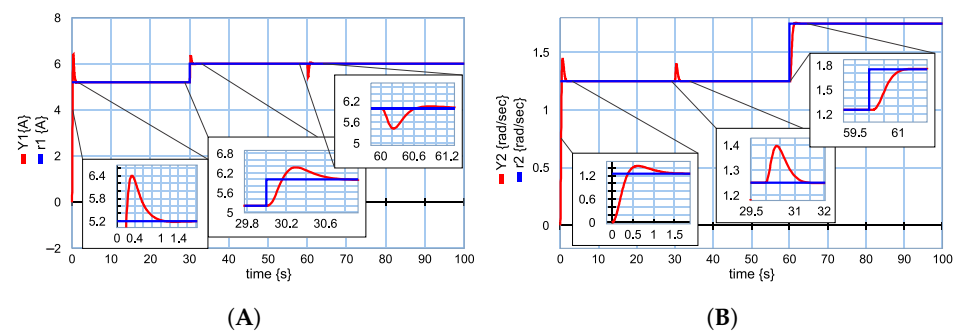


Figure 34. System outputs with a step tracking control with all eigenvalues at -10 : (A) Input r_1 and output y_1 ; (B) Input r_2 and output y_2 .

6.2. Ramp Tracking Control

The second tracking control to design is with an input command vector for constant ramps defined by

$$\begin{bmatrix} r_1(t) \\ r_2(t) \end{bmatrix} = \begin{bmatrix} r_{01} + r_{11} * t \\ r_{02} + r_{12} * t \end{bmatrix} \quad (76)$$

For this command input comparing (2) and (76), $\delta = 2$, then Procedure 1 is applied, and Figure 35 shows the open loop tracking system in a bond graph approach.

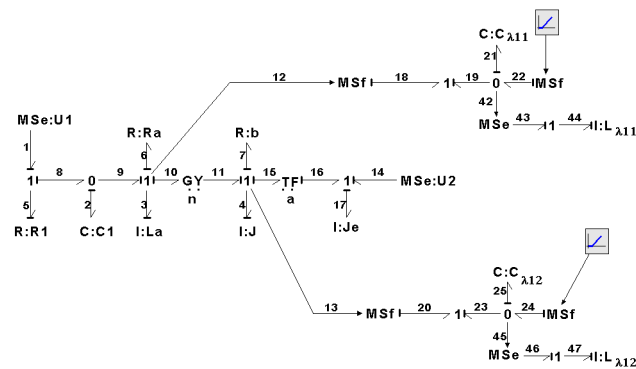


Figure 35. Open loop tracking system for ramps.

From Figure 12, introducing the storage elements ($I : L_{\lambda 11}$ and $I : L_{\lambda 12}$) whose bonds are (44 and 47), respectively, with their effort sources according to step 4 of Procedure 1, the bond graph in open loop for the ramp tracking control is built. The key vectors of the additional states for this bond graph are defined by

$$\lambda_1 = \begin{bmatrix} q_{21} \\ q_{25} \end{bmatrix}; \dot{\lambda}_1 = \begin{bmatrix} f_{21} \\ f_{25} \end{bmatrix}; \sigma_1 = \begin{bmatrix} e_{21} \\ e_{25} \end{bmatrix}$$

$$\lambda_2 = \begin{bmatrix} p_{44} \\ p_{47} \end{bmatrix}; \dot{\lambda}_2 = \begin{bmatrix} e_{44} \\ e_{47} \end{bmatrix}; \sigma_2 = \begin{bmatrix} f_{44} \\ f_{47} \end{bmatrix}; r = \begin{bmatrix} f_{22} \\ f_{24} \end{bmatrix}$$

The junction structure of the open loop system is given by

$$\begin{bmatrix} f_2 \\ e_3 \\ e_4 \\ e_5 \\ f_6 \\ f_7 \\ f_3 \\ f_4 \\ f_{17} \\ f_{21} \\ f_{25} \\ e_{44} \\ e_{47} \end{bmatrix} = \begin{bmatrix} 0 & -1 & 0 & 1 & 0 & 0 & 0 & 0 & 0 & 0 & 0 & 0 & 0 & 0 & 0 & 0 & 0 & 0 \\ 1 & 0 & -n & 0 & -1 & 0 & 0 & 0 & 0 & 0 & 0 & 0 & 0 & 0 & 0 & 0 & 0 & 0 \\ 0 & n & 0 & 0 & 0 & -1 & 0 & a & -a & 0 & 0 & 0 & 0 & 0 & 0 & 0 & 0 & 0 \\ \hline -1 & 0 & 0 & 0 & 0 & 0 & 1 & 0 & 0 & 0 & 0 & 0 & 0 & 0 & 0 & 0 & 0 & 0 \\ 0 & 1 & 0 & 0 & 0 & 0 & 0 & 0 & 0 & 0 & 0 & 0 & 0 & 0 & 0 & 0 & 0 & 0 \\ 0 & 0 & 1 & 0 & 0 & 0 & 0 & 0 & 0 & 0 & 0 & 0 & 0 & 0 & 0 & 0 & 0 & 0 \\ \hline 0 & 1 & 0 & 0 & 0 & 0 & 0 & 0 & 0 & 0 & 0 & 0 & 0 & 0 & 0 & 0 & 0 & 0 \\ 0 & 0 & 1 & 0 & 0 & 0 & 0 & 0 & 0 & 0 & 0 & 0 & 0 & 0 & 0 & 0 & 0 & 0 \\ \hline 0 & 0 & a & 0 & 0 & 0 & 0 & 0 & 0 & 0 & 0 & 0 & 0 & 0 & 0 & 0 & 0 & 0 \\ \hline 0 & -1 & 0 & 0 & 0 & 0 & 0 & 0 & 0 & 1 & 0 & 0 & 0 & 0 & 0 & 0 & 0 & 0 \\ 0 & 0 & -1 & 0 & 0 & 0 & 0 & 0 & 0 & 0 & 1 & 0 & 0 & 0 & 0 & 0 & 0 & 0 \\ 0 & 0 & 0 & 0 & 0 & 0 & 0 & 0 & 0 & 0 & 0 & \frac{1}{C_{\lambda 11}} & 0 & 0 & 0 & 0 & 0 & 0 \\ 0 & 0 & 0 & 0 & 0 & 0 & 0 & 0 & 0 & 0 & 0 & 0 & \frac{1}{C_{\lambda 12}} & 0 & 0 & 0 & 0 & 0 \end{bmatrix} \begin{bmatrix} e_2 \\ f_3 \\ f_4 \\ f_5 \\ e_6 \\ e_7 \\ e_1 \\ e_{14} \\ e_{17} \\ f_{22} \\ f_{24} \\ e_{21} \\ e_{25} \\ f_{44} \\ f_{47} \end{bmatrix} \quad (77)$$

The feedback control of system states (q_2, p_3, p_4) and of the additional states for tracking ($q_{21}, q_{25}, p_{44}, p_{47}$) is described by

$$\begin{bmatrix} u_1 \\ u_2 \end{bmatrix} = \begin{bmatrix} (K_x)_{11} & (K_x)_{12} & (K_x)_{13} & (K_{\lambda 1})_{11} & (K_{\lambda 1})_{12} & (K_{\lambda 2})_{13} & (K_{\lambda 2})_{14} \\ 0 & 0 & 0 & 0 & 0 & (K_{\lambda 2})_{23} & 0 \end{bmatrix} \begin{bmatrix} q_2 \\ p_3 \\ p_4 \\ q_{21} \\ q_{25} \\ p_{44} \\ p_{47} \end{bmatrix} \quad (78)$$

Applying step 5 of Procedure 1 to the bond graph of Figure 35, the closed loop tracking system for ramp and step inputs in the physical domain is built as shown in Figure 36.

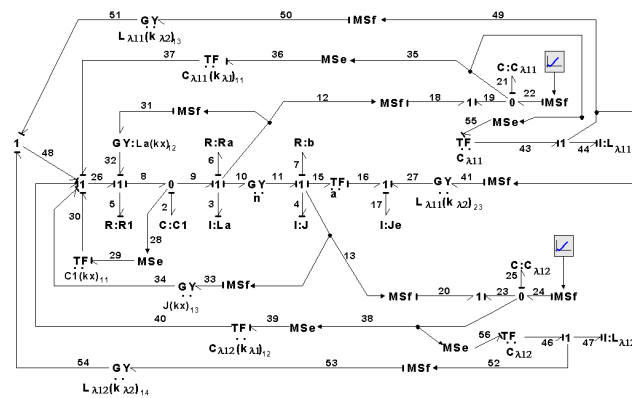


Figure 36. Closed loop tracking system for ramps.

The characteristic polynomial of the system has to be determined for the design of the control gains expressed by

$$s^7 + c_1 s^6 + c_2 s^5 + c_3 s^4 + c_4 s^3 + c_5 s^2 + c_6 s + c_7 = 0 \quad (79)$$

The coefficients of this polynomial using causal paths are defined by

- For c_1

$$c_1 = b_1 \quad (80)$$

- For c_2

$$c_2 = b_2 \quad (81)$$

- For c_3

- $(R : R_1 \longleftrightarrow C : C_1)$ and $[(I : L_a \longleftrightarrow R : R_a) \text{ and } (I : J \longleftrightarrow I : J_e)]$ given by (62)
- $(R : R_1 \longleftrightarrow C : C_1)$, $[(I : L_a \longleftrightarrow R : R_a) \text{ and } (I : J \longleftrightarrow R : b)]$ given by (63)
- $(I : L_a \longleftrightarrow C : C_1)$ and $(I : J \longleftrightarrow R : b)$ given by (64)
- $(I : J \longleftrightarrow I : J)$ given by (65)
- $(C : C_{\lambda 11} \longleftrightarrow I : L_a)$ given by (66)

$$\begin{aligned} c_3 &= a_3 - \frac{(k_x)_{11} n^2}{R_1 L_a \Lambda} - \frac{(k_x)_{11} R_a b}{R_1 L_a \Lambda} - \frac{(k_x)_{12} b}{R_1 C_1 \Lambda} - \frac{(k_{\lambda 1})_{11}}{R_1 C_1 L_a} - \frac{J n (k_x)_{13}}{R_1 C_1 L_a \Lambda} - \frac{a n (k_{\lambda 1})_{21}}{L_a \Lambda} \\ &= b_3 + \frac{a n (k_{\lambda 1})_{21}}{L_a \Lambda} \end{aligned} \quad (82)$$

- For c_4

- $(C : C_{\lambda 11} \longleftrightarrow C : C_{\lambda 11})$ and $(I : J \longleftrightarrow R : b)$ given by (69) with

$$C_{\lambda 11} (k_{\lambda 1})_{11} L_a (T) = \frac{(k_{\lambda 1})_{11}}{R_1 C_1 L_a} \cdot \frac{b}{\Lambda} \quad (83)$$

- $(I : L_{\lambda 11} \longleftrightarrow I : L_{\lambda 11})$ the causal loop is $(44 - 49 - 50 - 51 - 48 - 26 - 5 - 5 - 8 - 2 - 2 - 9 - 3 - 3 - 12 - 18 - 19 - 21 - 21 - 35 - 55 - 43 - 44)$ with

$$L_{\lambda 11} (k_{\lambda 2})_{13} L_a (T) = \frac{(k_{\lambda 2})_{13}}{R_1 C_1 L_a} \quad (84)$$

The causal loops of terms (83) and (84) are shown in Figure 37.

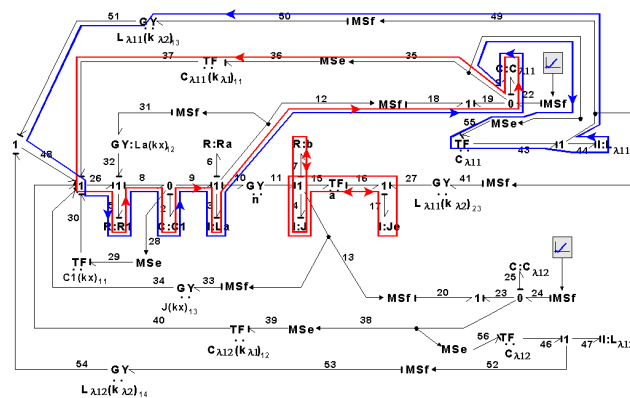


Figure 37. Causal loops for (83) and (84).

- $(C : C_{\lambda 12} \longleftrightarrow C : C_{\lambda 12})$ the causal loop is $(25 - 38 - 39 - 40 - 26 - 55 - 8 - 2 - 2 - 9 - 3 - 3 - 10 - 11 - 4 - 4 - 13 - 20.23 - 25)$ with

$$C_{\lambda 12}(k_{\lambda 1})_{12} L_a(T) = - \frac{n(k_{\lambda 1})_{12}}{R_1 C_1 L_a \Lambda} \quad (85)$$

- $(I : L_{\lambda 11} \longleftrightarrow I : L_{\lambda 11})$ the causal loop is $(44 - 41 - 27 - 16 - 15 - 4 - 4 - 11 - 10 - 3 - 3 - 12 - 18 - 19 - 21 - 21 - 35 - 55 - 43 - 44)$ with

$$L_{\lambda 11}(k_{\lambda 2})_{23} L_a(T) = - \frac{an(k_{\lambda 2})_{23}}{L_a \Lambda} \quad (86)$$

The causal loops of terms (85) and (86) are illustrated in Figure 38.

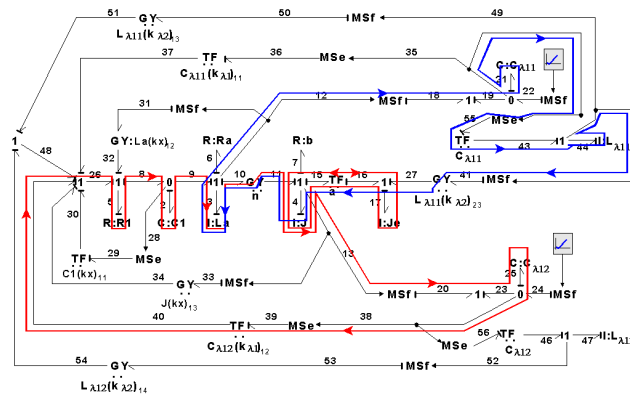


Figure 38. Causal loops for (85) and (86).

- then

$$c_4 = \frac{C_{\lambda 11}(k_{\lambda 1})_{11} L_a(T) + C_{\lambda 12}(k_{\lambda 1})_{12} L_a(T) + L_{\lambda 11}(k_{\lambda 2})_{13} L_a(T) + L_{\lambda 11}(k_{\lambda 2})_{23} L_a(T)}{JbJ_e} \quad (87)$$

$$c_4 = \frac{b(k_{\lambda 1})_{11}}{R_1 C_1 L_a \Lambda} - \frac{n(k_{\lambda 1})_{12}}{R_1 C_1 L_a \Lambda} + \frac{(k_{\lambda 2})_{13}}{R_1 C_1 L_a} - \frac{an(k_{\lambda 2})_{23}}{L_a \Lambda}$$

- For c_5

- $(I : L_{\lambda 11} \longleftrightarrow I : L_{\lambda 11})$ and $(I : J \longleftrightarrow R : b)$ given by (84) and (39), respectively

$$L_{\lambda 11}(k_{\lambda 2})_{13} L_a(T) = \frac{(k_{\lambda 2})_{13}}{R_1 C_1 L_a} \cdot \frac{b}{\Lambda} \quad (88)$$

- $(I : L_{\lambda 11} \longleftrightarrow I : L_{\lambda 11})$ and $(C : C_1 \longleftrightarrow R : R_1)$ given by (86) and (35), respectively

$$\frac{L_{\lambda 11}(k_{\lambda 2})_{23} L_a}{J b I_e}(T)^{R_1 C_1} = -\frac{a n(k_{\lambda 2})_{23}}{L_a \Lambda} \cdot \frac{1}{R_1 C_1} \quad (89)$$

The causal loops of terms (88) and (89) are shown in Figure 39.

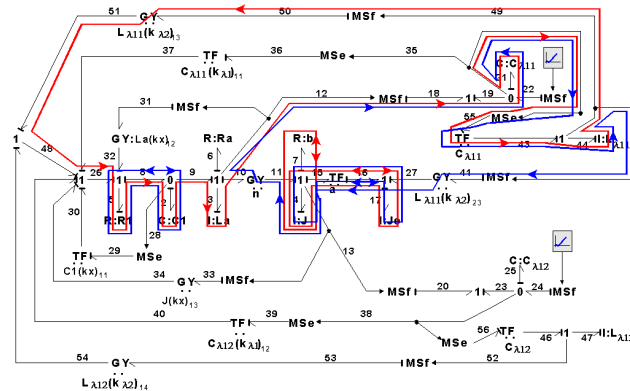


Figure 39. Causal loops for (88) and (89).

- – $(C : C_{\lambda 12} \longleftrightarrow C : C_{\lambda 12})$ the causal path is (25 – 38 – 56 – 46 – 47 – 47 – 52 – 53 – 54 – 48 – 26 – 5 – 5 – 8 – 2 – 2 – 9 – 3 – 3 – 10 – 11 – 4 – 4 – 13 – 20 – 23 – 25)

$$C_{\lambda 12}(k_{\lambda 2})_{14} I(T) = \frac{(k_{\lambda 2})_{14}}{R_1 C_1 L_a} \cdot \frac{n}{\Lambda} \quad (90)$$

- $(I : L_{\lambda 11} \longleftrightarrow I : L_{\lambda 11})$ the causal path is (44 – 49 – 41 – 27 – 16 – 15 – 4 – 4 – 11 – 10 – 3 – 3 – 9 – 2 – 2 – 28 – 29 – 30 – 26 – 5 – 5 – 8 – 2 – 2 – 9 – 3 – 3 – 12 – 18 – 19 – 21 – 21 – 35 – 55 – 43 – 44) with

$$L_{\lambda 11}(k_{\lambda 2})_{23} L_a(k_x)_{11}(T) = \frac{a n(k_x)_{11}(k_{\lambda 2})_{23}}{R_1 L_a \Lambda} \quad (91)$$

The causal loops of terms (90) and (91) are illustrated in Figure 40.

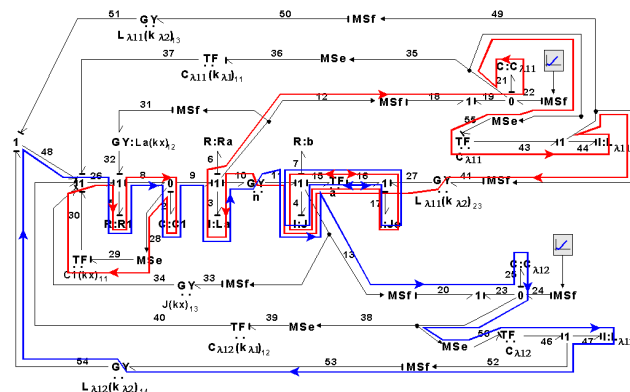


Figure 40. Causal loops for (90) and (91).

- – $(I : L_{\lambda 11} \longleftrightarrow I : L_{\lambda 11})$ the causal path is (44 – 49 – 41 – 27 – 17 – 17 – 16 – 15 – 14 – 4 – 13 – 33 – 34 – 26 – 5 – 5 – 8 – 2 – 2 – 9 – 3 – 3 – 12 – 18 – 19 – 21 – 21 – 35 – 55 – 43 – 44) with

$$\frac{L_{\lambda 11}(k_{\lambda 2})_{23} L_a}{J b I_e}(T) = \frac{a(k_x)_{13}(k_{\lambda 2})_{23} I}{R_1 C_1 L_a \Lambda} \quad (92)$$

The causal loops of term (92) can be seen in Figure 41.

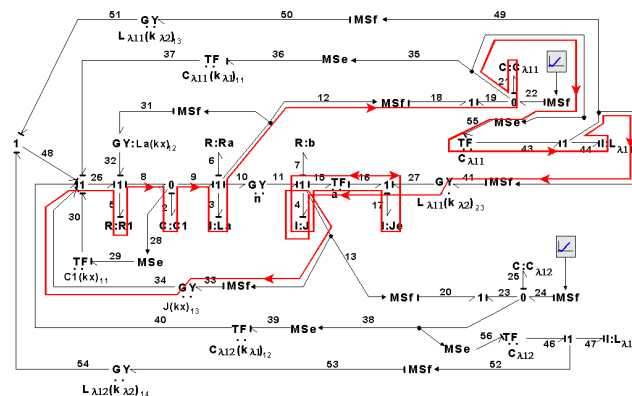


Figure 41. Causal loops for (92).

- – Then

$$c_5 = \frac{a(k_x)_{13}(k_{\lambda 2})_{23}I}{R_1 C_1 L_a \Lambda} + \frac{an(k_x)_{11}(k_{\lambda 2})_{23}}{R_1 L_a \Lambda} + \frac{b(k_{\lambda 2})_{13}}{R_1 C_1 L_a \Lambda} + \frac{n(k_{\lambda 2})_{14}}{R_1 C_1 L_a \Lambda} - \frac{an(k_{\lambda 2})_{23}}{R_1 C_1 L_a \Lambda} \quad (93)$$

- For c_6 , the only term of this factor has the causal path (25 – 38 – 39 – 40 – 26 – 5 – 5 – 8 – 2 – 2 – 9 – 3 – 3 – 12 – 18 – 19 – 21 – 21 – 35 – 55 – 43 – 44 – 41 – 27 – 17 – 17 – 16 – 15 – 4 – 4 – 13 – 20 – 23 – 25) with

$$c_6 = \frac{-a(k_{\lambda 1})_{12}(k_{\lambda 2})_{23}}{R_1 C_1 L_a \Lambda} \quad (94)$$

which is shown in Figure 42.

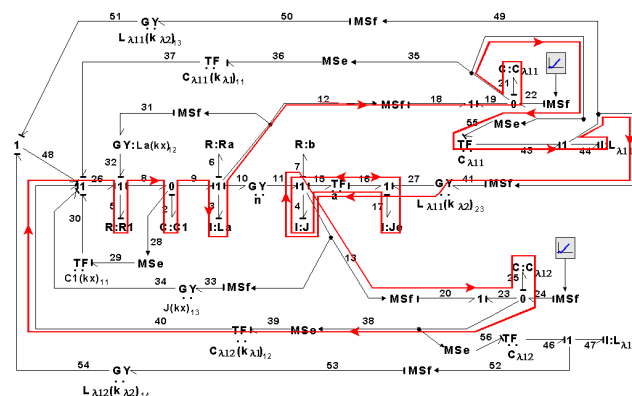


Figure 42. Causal loops for c_6 .

- For c_7 , the only term of this factor has the causal path (25 – 38 – 56 – 46 – 47 – 47 – 52 – 53 – 54 – 48 – 26 – 5 – 5 – 8 – 2 – 2 – 9 – 3 – 3 – 12 – 18 – 19 – 21 – 21 – 35 – 55 – 43 – 44 – 44 – 41 – 27 – 17 – 17 – 16 – 15 – 4 – 4 – 13 – 20 – 23 – 25) with

$$c_7 = \frac{-a(k_{\lambda 2})_{14}(k_{\lambda 2})_{23}}{R_1 C_1 L_a \Lambda} \quad (95)$$

and it is shown in Figure 43.

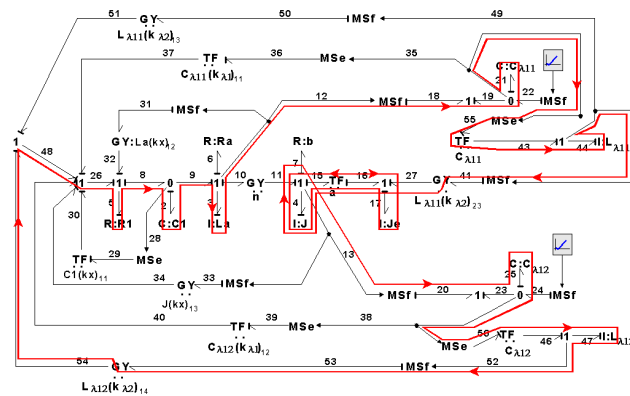


Figure 43. Causal loops for c_7 .

The gains for this tracking control considering that all the eigenvalues are at -1 are given in Table 6.

Table 6. Gains for the ramp tracking controller with eigenvalues at -1 .

$(k_x)_{11} = 60.8$	$(k_x)_{12} = 197.52$	$(k_x)_{13} = 0.1984$	$(k_{\lambda 1})_{11} = 0.026512$
$(k_{\lambda 1})_{12} = -0.28$	$(k_{\lambda 2})_{13} = 0.0064128$	$(k_{\lambda 2})_{14} = -0.04$	$(k_{\lambda 2})_{23} = 0.01$

Figure 44 shows the performance of the tracking control in the physical domain. The tracking input for the current signal in this simulation case is of the form $r_1(t) = 0.5 * t$ ($0 \leq t \leq 30$ s). From 30 to 60 s, there is a negative slope of 0.5 resulting in a constant step signal of 15 A; for $t > 60$ s the current signal to track is with a slope of 1.5, i.e., $r_1(t) = 1.5 * t$. The tracking input for the torque signal is $r_2(t) = 0.2 * t$ ($0 \leq t \leq 85$ s) and $r_2(t) = -0.5 * t$ ($85 < t < \infty$).

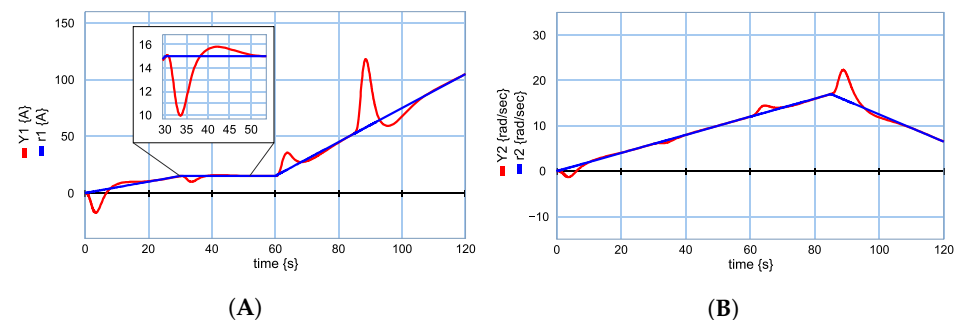


Figure 44. System outputs with a ramp tracking control with all eigenvalues at -1 : (A) Input r_1 and output y_2 ; (B) Input r_2 and output y_2 .

Now, considering all eigenvalues at -10 , the controller gains are indicated in Table 7.

Table 7. Gains for the ramp tracking controller with eigenvalues at -10 .

$(k_x)_{11} = -65.2$	$(k_x)_{12} = 145.61$	$(k_x)_{13} = 14.931$	$(k_{\lambda 1})_{11} = 13.29$
$(k_{\lambda 1})_{12} = -28$	$(k_{\lambda 2})_{13} = 114.1$	$(k_{\lambda 2})_{14} = -40$	$(k_{\lambda 2})_{23} = 100$

Figure 45 illustrates the effectiveness of the controller with the given conditions.

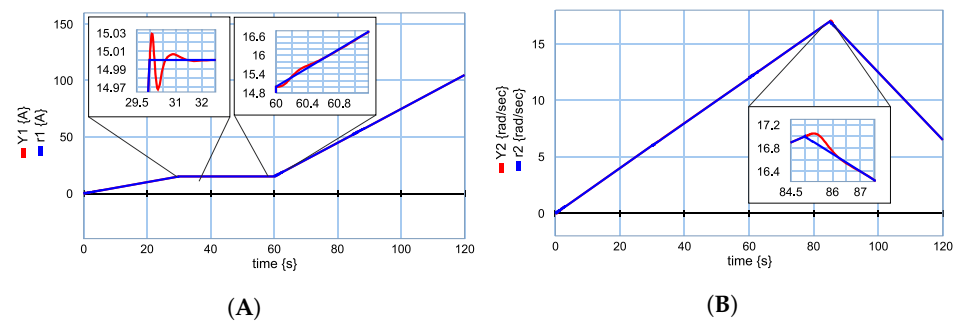


Figure 45. System outputs with a ramp tracking control with all eigenvalues at -10 : (A) Input r_1 and output y_1 ; (B) Input r_2 and output y_2 .

Figures 44 and 45 show that the DC motor outputs can effectively track the desired ramp inputs. In order to stabilize the output responses at shorter times, the eigenvalues of -1 in Figure 44 are changed to -10 in Figure 45. In addition, the desired ramp inputs can have steps.

6.3. Acceleration Tracking Control

The last tracking control is of the acceleration shape defined by

$$\begin{bmatrix} r_1(t) \\ r_2(t) \end{bmatrix} = \begin{bmatrix} r_{01} + r_{11} * t + r_{21} * t^2 \\ r_{02} + r_{12} * t + r_{22} * t^2 \end{bmatrix} \quad (96)$$

for this signal; according to (2) and (96), it results $\delta = 3$. The open loop system is built by adding storage elements ($C : C_{\lambda 21}$ and $C : C_{\lambda 22}$) whose bonds are (59 and 62), respectively, according to step 4 of Procedure 1, which is shown in Figure 46.

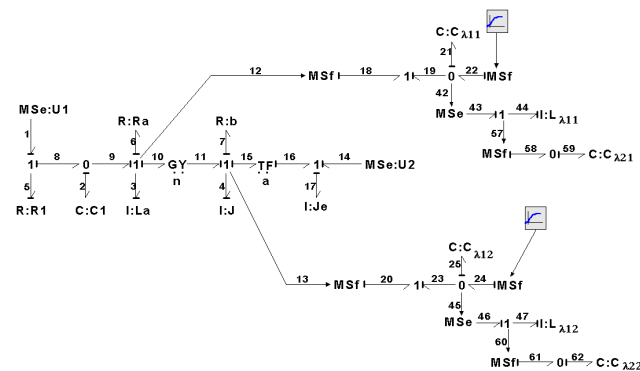


Figure 46. Open loop tracking system for accelerations.

The key vectors for the additional states of the bond graph are defined by

$$\begin{aligned} \lambda_1 &= \begin{bmatrix} q_{21} \\ q_{25} \end{bmatrix}; \dot{\lambda}_1 = \begin{bmatrix} f_{21} \\ f_{25} \end{bmatrix}; \sigma_1 = \begin{bmatrix} e_{21} \\ e_{25} \end{bmatrix} \\ \lambda_2 &= \begin{bmatrix} p_{44} \\ p_{47} \end{bmatrix}; \dot{\lambda}_2 = \begin{bmatrix} e_{44} \\ e_{47} \end{bmatrix}; \sigma_2 = \begin{bmatrix} f_{44} \\ f_{47} \end{bmatrix} \\ \lambda_3 &= \begin{bmatrix} q_{59} \\ q_{62} \end{bmatrix}; \dot{\lambda}_3 = \begin{bmatrix} f_{59} \\ f_{62} \end{bmatrix}; \sigma_3 = \begin{bmatrix} e_{59} \\ e_{62} \end{bmatrix}; r = \begin{bmatrix} f_{22} \\ f_{24} \end{bmatrix} \end{aligned}$$

The junction structure of the open loop system is given by

$$\begin{bmatrix} f_2 \\ e_3 \\ e_4 \\ e_5 \\ f_6 \\ f_7 \\ f_3 \\ f_4 \\ f_{17} \\ f_{21} \\ f_{25} \\ e_{44} \\ e_{47} \\ f_{59} \\ f_{62} \end{bmatrix} = \begin{bmatrix} 0 & -1 & 0 & 1 & 0 & 0 & 0 & 0 & 0 & 0 & 0 & 0 & 0 & 0 & 0 & 0 \\ 1 & 0 & -n & 0 & -1 & 0 & 0 & 0 & 0 & 0 & 0 & 0 & 0 & 0 & 0 & 0 \\ 0 & n & 0 & 0 & 0 & -1 & 0 & a & -a & 0 & 0 & 0 & 0 & 0 & 0 & 0 \\ \hline -1 & 0 & 0 & 0 & 0 & 0 & 1 & 0 & 0 & 0 & 0 & 0 & 0 & 0 & 0 & 0 \\ 0 & 1 & 0 & 0 & 0 & 0 & 0 & 0 & 0 & 0 & 0 & 0 & 0 & 0 & 0 & 0 \\ 0 & 0 & 1 & 0 & 0 & 0 & 0 & 0 & 0 & 0 & 0 & 0 & 0 & 0 & 0 & 0 \\ \hline 0 & 1 & 0 & 0 & 0 & 0 & 0 & 0 & 0 & 0 & 0 & 0 & 0 & 0 & 0 & 0 \\ 0 & 0 & 1 & 0 & 0 & 0 & 0 & 0 & 0 & 0 & 0 & 0 & 0 & 0 & 0 & 0 \\ \hline 0 & 0 & a & 0 & 0 & 0 & 0 & 0 & 0 & 0 & 0 & 0 & 0 & 0 & 0 & 0 \\ \hline 0 & -1 & 0 & 0 & 0 & 0 & 0 & 0 & 1 & 0 & 0 & 0 & 0 & 0 & 0 & 0 \\ 0 & 0 & -1 & 0 & 0 & 0 & 0 & 0 & 0 & 1 & 0 & 0 & 0 & 0 & 0 & 0 \\ 0 & 0 & 0 & 0 & 0 & 0 & 0 & 0 & 0 & 0 & \frac{1}{C_{\lambda 11}} & 0 & 0 & 0 & 0 & 0 \\ 0 & 0 & 0 & 0 & 0 & 0 & 0 & 0 & 0 & 0 & 0 & \frac{1}{C_{\lambda 12}} & 0 & 0 & 0 & 0 \\ 0 & 0 & 0 & 0 & 0 & 0 & 0 & 0 & 0 & 0 & 0 & 0 & \frac{1}{L_{\lambda 11}} & 0 & 0 & 0 \\ 0 & 0 & 0 & 0 & 0 & 0 & 0 & 0 & 0 & 0 & 0 & 0 & 0 & \frac{1}{L_{\lambda 12}} & 0 & 0 \end{bmatrix} \begin{bmatrix} e_2 \\ f_3 \\ f_4 \\ f_5 \\ e_6 \\ e_7 \\ e_1 \\ e_{14} \\ e_{17} \\ f_{22} \\ f_{24} \\ e_{21} \\ e_{25} \\ f_{44} \\ f_{47} \\ e_{59} \\ e_{62} \end{bmatrix} \quad (97)$$

Feedback gains to achieve signal tracking are of the form

$$\begin{bmatrix} u_1 \\ u_2 \end{bmatrix} = \begin{bmatrix} (k_x)_{11} & (k_x)_{12} & (k_x)_{13} \\ 0 & 0 & 0 \end{bmatrix} \begin{bmatrix} q_2 \\ p_3 \\ p_4 \end{bmatrix} + \quad (98)$$

$$\begin{bmatrix} (k_{\lambda 1})_{11} & (k_{\lambda 1})_{12} & (k_{\lambda 2})_{13} & (k_{\lambda 2})_{14} & (k_{\lambda 3})_{15} & (k_{\lambda 3})_{16} \\ 0 & 0 & 0 & 0 & (k_{\lambda 3})_{25} & 0 \end{bmatrix} \begin{bmatrix} q_{21} \\ q_{25} \\ p_{44} \\ p_{47} \\ q_{59} \\ q_{62} \end{bmatrix}$$

Adding the feedback gains (98) according to step 5 of Procedure 1, the bond graph of the closed loop system is illustrated in Figure 47.

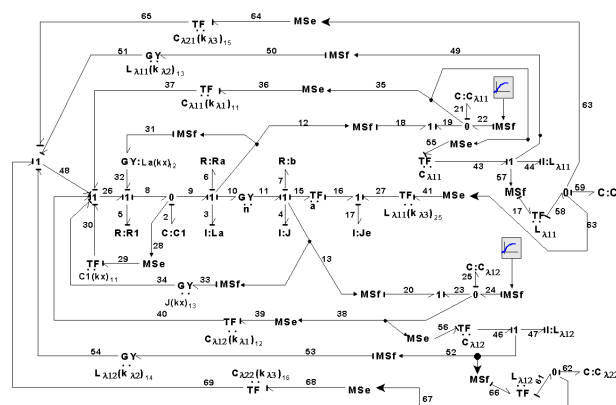


Figure 47. Closed loop tracking system for accelerations.

The polynomial characteristic of this system is expressed by

$$s^9 + d_1 s^8 + d_2 s^7 + d_3 s^6 + d_4 s^5 + d_5 s^4 + d_6 s^3 + d_7 s^2 + d_8 s + d_9 = 0 \quad (99)$$

The coefficients of (99) are calculated by

$$d_1 = b_1 \quad (100)$$

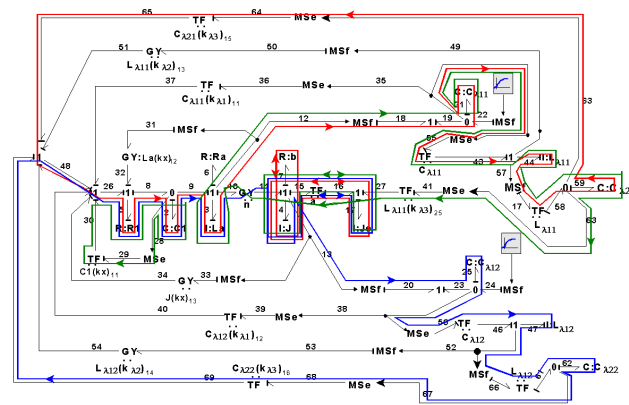


Figure 50. Causal loops for (107), (108), and (109).

- $(C : C_1 \longleftrightarrow R : R_1)$ given by (35) and $(C : C_{\lambda 21} \longleftrightarrow C : C_{\lambda 21})$; the causal path is $(59 - 63 - 41 - 27 - 16 - 15 - 4 - 4 - 11 - 10 - 3 - 3 - 12 - 18 - 19 - 21 - 21 - 35 - 55 - 43 - 44 - 44 - 57 - 17 - 58 - 59)$ with

$$\frac{C_{\lambda 21}(k_{\lambda 3})_{15} L_a(T)}{R_1 C_1} = \frac{-an(k_{\lambda 3})_{25}}{L_a \Lambda} \cdot \frac{1}{R_1 C_1} \quad (110)$$

- $(C : C_{\lambda 21} \longleftrightarrow C : C_{\lambda 21})$ the causal path is $(59 - 63 - 41 - 27 - 16 - 15 - 4 - 4 - 11 - 10 - 3 - 3 - 9 - 2 - 2 - 28 - 29 - 30 - 26 - 5 - 5 - 8 - 2 - 2 - 9 - 3 - 3 - 12 - 18 - 19 - 21 - 21 - 35 - 55 - 43 - 44 - 44 - 57 - 17 - 58 - 59)$ with

$$C_{\lambda 21}(k_{\lambda 3})_{25}(k_x)_{11}(T) = \frac{an(k_x)_{11}(k_{\lambda 3})_{25}}{R_1 L_a \Lambda} \quad (111)$$

Figure 51 shows the unidirectional causal loops of terms (110) and (111).

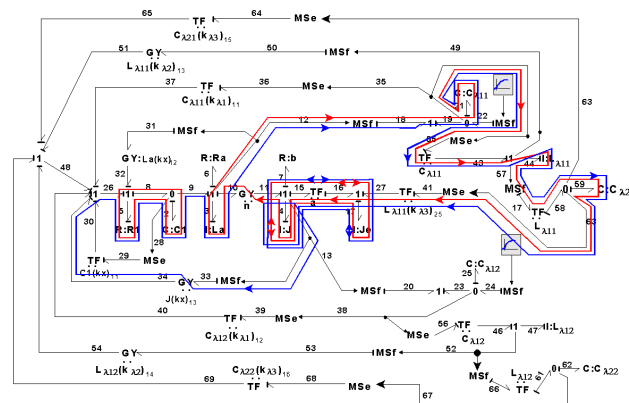


Figure 51. Causal loops for (110) and (111).

- Then

$$d_6 = \frac{b(k_{\lambda 3})_{15}}{R_1 C_1 L_a \Lambda} + \frac{n(k_{\lambda 3})_{16}}{R_1 C_1 L_a \Lambda} - \frac{an(k_{\lambda 3})_{25}}{R_1 C_1 L_a \Lambda} + \frac{a(k_x)_{13}(k_{\lambda 3})_{25} I}{R_1 C_1 L_a \Lambda} + \frac{an(k_x)_{11}(k_{\lambda 3})_{25}}{R_1 L_a \Lambda} \quad (112)$$

- For d_7 , the only term of this factor $(C : C_{\lambda 21} \longleftrightarrow C : C_{\lambda 21})$ has the causal path $(59 - 63 - 41 - 27 - 16 - 15 - 4 - 4 - 13 - 20 - 23 - 25 - 25 - 38 - 39 - 40 - 26 - 5 - 5 - 8 - 2 - 2 - 9 - 3 - 3 - 12 - 18 - 19 - 21 - 21 - 35 - 55 - 43)$

−44 − 44 − 57 − 17 − 58 − 59) with

$$d_7 = \frac{-a(k_{\lambda 1})_{12}(k_{\lambda 3})_{25}}{R_1 C_1 L_a \Lambda} \quad (113)$$

This term is shown in Figure 52.

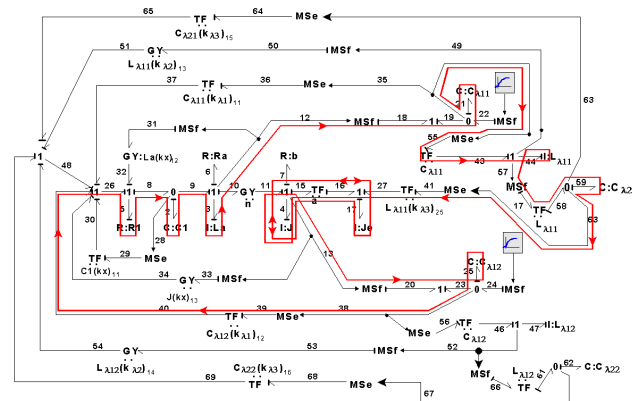


Figure 52. Causal loops for d_7 .

- For d_8 , the only term of this factor ($C : C_{\lambda 21} \longleftrightarrow C : C_{\lambda 21}$) has the causal path (59 − 63 − 41 − 27 − 16 − 15 − 4 − 4 − 13 − 20 − 23 − 25 − 25 − 38 − 56 − 46 − 47 − 47 − 52 − 53 − 54 − 48 − 26 − 5 − 5 − 8 − 2 − 2 − 9 − 3 − 3 − 12 − 18 − 19 − 21 − 21 − 35 − 55 − 43 − 44 − 57 − 17 − 58 − 59) with

$$d_8 = \frac{-a(k_{\lambda 2})_{14}(k_{\lambda 3})_{25}}{R_1 C_1 L_a \Lambda} \quad (114)$$

and it is illustrated in Figure 53.

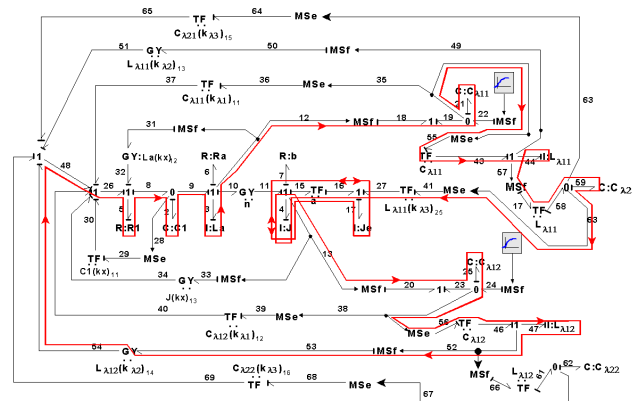


Figure 53. Causal loops for d_8 .

- For d_9 , the only term of this factor ($C : C_{\lambda 21} \longleftrightarrow C : C_{\lambda 21}$) has the causal path (59 − 63 − 41 − 27 − 16 − 15 − 4 − 4 − 13 − 20 − 23 − 25 − 25 − 38 − 56 − 46 − 47 − 47 − 52 − 66 − 61 − 62 − 67 − 68 − 69 − 48 − 26 − 5 − 5 − 8 − 2 − 2 − 9 − 3 − 3 − 12 − 18 − 19 − 21 − 21 − 35 − 55 − 43 − 44 − 57 − 17 − 58 − 59) with

$$d_9 = \frac{-a(k_{\lambda 3})_{16}(k_{\lambda 3})_{25}}{R_1 C_1 L_a \Lambda} \quad (115)$$

which is shown in Figure 54.

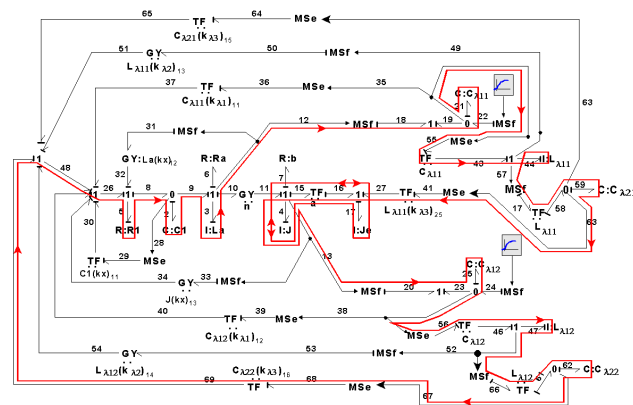


Figure 54. Causal loops for d_9 .

The determination of the gains for the location of the eigenvalues at -1 is given in Table 8.

Table 8. Gains for the acceleration tracking controller with eigenvalues at -1 .

$(k_x)_{11} = 56.8$	$(k_x)_{12} = 197.91$	$(k_x)_{13} = 13.454$	$(k_{\lambda 1})_{11} = 1.0951$	$(k_{\lambda 1})_{12} = -14.4$
$(k_{\lambda 2})_{13} = 0.30222$	$(k_{\lambda 2})_{14} = -3.6$	$(k_{\lambda 3})_{15} = 0.045087$	$(k_{\lambda 3})_{16} = -0.4$	$(k_{\lambda 3})_{25} = 0.001$

The acceleration signals for current and torque in this tracking control are

$$r_1(t) = 0.002 + 0.15 * t + 0.05 * t^2$$

$$r_2(t) = 0.5 + 0.12 * t + 0.2 * t^2$$

The dynamic behavior of the system outputs is shown in Figure 55. In this case, the convergence to the reference signals is relatively slow.

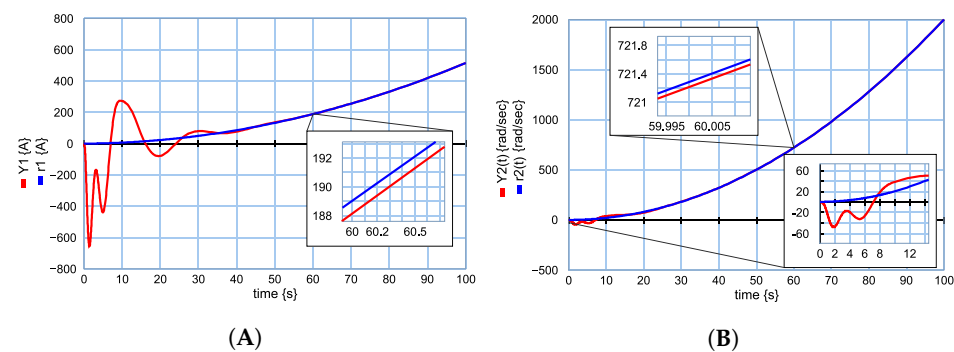


Figure 55. System outputs with an acceleration tracking control with all eigenvalues at -1 : (A) Input r_1 and output y_1 ; (B) Input r_2 and output y_2 .

For a faster response of the control, the location of the eigenvalues at -10 is proposed where Table 9 gives the values of the feedback gains and Figure 56 gives the performance of the outputs.

Table 9. Gains for the acceleration tracking controller with eigenvalues at -1 .

$(k_x)_{11} = -105.2$	$(k_x)_{12} = 95.530$	$(k_x)_{13} = 60.737$	$(k_{\lambda 1})_{11} = 35.145$	$(k_{\lambda 1})_{12} = -144$
$(k_{\lambda 2})_{13} = 448.46$	$(k_{\lambda 2})_{14} = -360$	$(k_{\lambda 3})_{15} = 4039.8$	$(k_{\lambda 3})_{16} = -400$	$(k_{\lambda 3})_{25} = 1000$

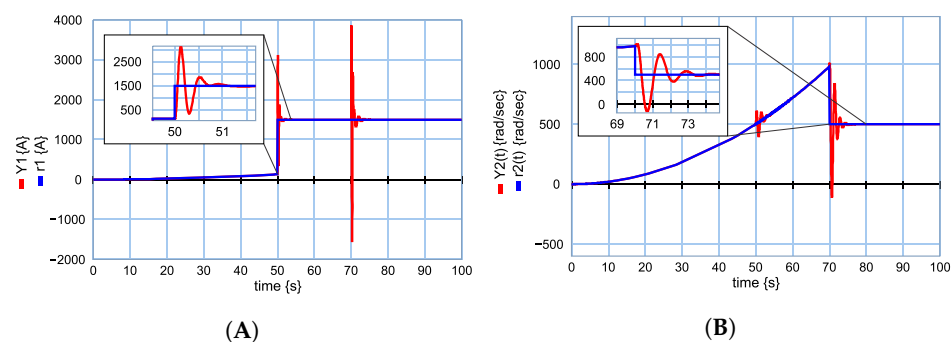


Figure 56. System outputs with an acceleration tracking control with all eigenvalues at -10 : (A) Input r_1 and output y_1 ; (B) Input r_2 and output y_2 .

Regarding control with acceleration tracking inputs for current and angular velocity whose responses are shown in Figures 55 and 56, it can be seen that the successful design of a bond graph of the closed loop system has been achieved. Due to the fact that general tracking inputs must be polynomial, different inputs can be proposed to know different performances of the system outputs. In addition, the controller designs in the bond graph for the step, ramp, and acceleration inputs differ in the increase of the storage elements that determine the additional state variables and the corresponding feedback gains.

Note that the proposed procedure is an interesting tool when an LTI system is modeled by a bond graph; then, the closed loop tracking system in a bond graph approach can be obtained in a direct way. This paper gives the possibility of having a closed loop tracking system of a real system and building the tracking system and the feedback gains with external elements to the system, and we can validate the method and models of this paper.

7. Conclusions

The extension of modeling of physical systems to their tracking control in a bond graph has been presented. An additional bond graph containing additional state variables and the feedback gains determine the proposed controller. The advantages of this approach are that it does not require the mathematical model of the system and it can control systems with different energy domains. In addition, linearly independent and dependent state variables are considered. Therefore, modeling and control symmetries between the bond graph and state space approaches have been established. A DC motor fed with an electrical network and with a mechanical load represents the case study in this paper. First, a tracking control with step signals is designed. From this controller, additional elements are introduced to track ramp type signals. Finally, this controller for acceleration signals is extended. In order to verify the effectiveness of the controllers simulation, results have been shown.

Author Contributions: Conceptualization, A.P.G. and G.G.-A.; methodology, A.P.G.; validation, N.B.G.; formal analysis, J.M.-B. and N.B.G.; writing—original draft preparation, A.P.G. and G.G.-A.; writing—review and editing, G.G.-A., G.A.-J., D.A.-Z. and A.P.G. All authors have read and agreed to the published version of the manuscript.

Funding: This research received no external funding.

Institutional Review Board Statement: Not applicable.

Informed Consent Statement: Not applicable.

Data Availability Statement: No other was used for this article.

Conflicts of Interest: The authors declare no conflict of interest.

Appendix A. Causal Paths

In this section, the definition and classification of the zero-causal paths [32] are described.

The classification of zero-order causal paths follows from the research work carried out by Van Dijk and Breedveld [32].

Definitions

Causal path is a sequence of causal bonds between two vertices of the bond graph. The causal strokes must be attached to each bond at the “same relative position”.

Causal cycle is a closed causal path.

Topological loop is a signal (flow or effort) loop associated with a causal cycle.

Causal mesh is a closed causal path, which usually ends in a port of an element, and it has to contain an odd number of gyrators.

A causal cycle is an *essential causal cycle* if:

1. There is a closed path along a simple junction structure. If more conservation principles than just power conservation are applicable, then the bond graph must represent them explicitly.
2. There is a closed causal path along a weighted junction structure, and the loop gain associated with this causal cycle is not equal to 1.

In all other cases, the causal cycle is not essential.

Zero-order causal path is a causal path with topological loops whose variables are related to themselves by means of algebraic assignments [32].

The following classification of zero-order causal can be described [32],

Class 1 zero-order causal path: causal path is between a storage element (or port) with a derivative and a storage element (port) with integral causality (Figure A1a).

Class 2 zero-order causal path: causal path is between elements (ports) whose constitutive relations are algebraic (algebraic loop) (Figure A1b).



Figure A1. Bond graphs with (a) class 1 and (b) class 2 zero-order causal paths.

Class 3 zero-order causal path: the closed causal path is an essential causal cycle (Figure A2a).

Class 4 zero-order causal path: causal cycle is not essential. The loop gain of the topological loops is always +1 (Figure A2b).

Class 5 zero-order causal path: the closed causal path is a causal mesh (Figure A2c).

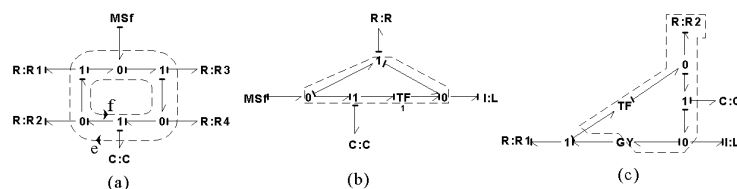


Figure A2. Bond graphs with (a) class 3, (b) class 4, and (c) class 5 zero-order causal paths.

References

1. Porter, B.; Bradshaw, A. Design of linear multivariable continuous-time tracking systems. *Int. Syst. Sci.* **1974**, *5*, 1156–1164. [\[CrossRef\]](#)
2. Young, P.C.; Willems, J.C. An approach to the linear multivariable servomechanism problem. *Int. Control* **1972**, *15*, 961–979. [\[CrossRef\]](#)
3. Osman, J.H.S.; Roberts, P.D. A class of Decentralized Tracking Controller for Robot Manipulators. *Proc. Inst. Mech. Eng. Part I J. Syst. Control Eng.* **1991**, *205*, 141–150. [\[CrossRef\]](#)
4. Ha, W.; Back, J. A Robust Tracking Controller for Robot Manipulators: Embedding Internal Model of Disturbances. In Proceedings of the IEEE International Conference on Robotics and Automation (ICRA), Montreal, QC, Canada, 20–24 May 2019. [\[CrossRef\]](#)

5. Hwang, C.L.; Lan, C.H.; Jieng, W.J. The trajectory tracking of an electrohydraulic servo-mechanism via a sliding mode controller. *Proc. Inst. Mech. Eng. Part I J. Systems Control Eng.* **1993**, *207*, 135–142. [\[CrossRef\]](#)
6. Ghazali, R.; Ngaden, R.; Sam, Y.M.; Rahmat, M.F.; Zulfatman; Hamzah, N. Chaotic trajectory tracking of an electron-hydraulic actuator system using discrete sliding mode control. In Proceedings of the IEEE International Conference on Control System, Computing and Engineering, Penang, Malaysia, 25–27 November 2011. [\[CrossRef\]](#)
7. Zhao, Z.M.; Yuan, X.Y.; Guo, Y.; Xu, F.; Li, Z.G. Modelling and simulation of a two-axis tracking system. *Proc. Inst. Mech. Eng. Part I J. Syst. Control Eng.* **2010**, *224*, 125–137 [\[CrossRef\]](#)
8. Cho, H.S.; Lee, C.W.; Cho, Y.J. Optimal control-system design for solar-tracking concentrators. *Trans. Inst. Meas. Control* **1980**, *2*, 207–213. [\[CrossRef\]](#)
9. Abadi, I.; Musyafa, A.; Soeprinanto, A. Design and Implementation of Active Two Axes Solar Tracking System Using Particle Swarm Optimizatgion Based Fuzzy Logic Controller. *Int. Model. Simul. (IREMOS)* **2015**, *8*, 640–652. [\[CrossRef\]](#)
10. Marcu, A.; Alexandru, C.; Barbu, I. Modeling and Simulation of a dual-axis solar tracker for PV modules. In Proceedings of the Product Design, Robotics, Advanced Mechanical and Mechatronic Systems and Innovation Conference (PRASIC), Brasov, Romania, 8–9 November 2018; IOP Conference Series: Materials Science and Engineering; Volume 514. [\[CrossRef\]](#)
11. Wu, J.; Wu, Z.-G.; Li, J.; Wang, G.; Zhao, H.; Chen, W. Practical Adaptive Fuzzy Control of Nonlinear Pure-feedback Systems with Quantized Nonlinearity Input. *IEEE Trans. Syst. Man Cybern. Syst.* **2019**, *49*, 638–648. [\[CrossRef\]](#)
12. Wu, J.; Chen, X.; Zhao, Q.; Li, J.; Wu, Z.-G. Adaptive Neural Dynamic Surface Control with Prespecified Tracking Accuracy of Uncertain Stochastic Nonstrict-Feedback Systems. *IEEE Trans. Cybern.* **2020**, 1–14. [\[CrossRef\]](#)
13. Karnopp, D.C.; Rosenberg, R.C. *Systems Dynamics: A Unified Approach*; Wiley John & Sons: Hoboken, NJ, USA, 1975.
14. Wellstead, P.E. *Physical System Modelling*; Academic Press: London, UK, 1979.
15. Silverman, L.M. Inversion of multivariable linear systems. *IEEE Trans. Autom. Control* **1969**, *AC-14*, 270–276. [\[CrossRef\]](#)
16. Pushkov, S.G. Inversion of Linear Systems on the Basis of State Space Realization. *J. Comput. Syst. Sci. Int.* **2018**, *57*, 7–17. [\[CrossRef\]](#)
17. Gawthrop, P.J. Bicausal bond graphs. In Proceedings of the 1995 International Conference on Bond Graph Modelling and Simulation: ICBGM'95, Las Vegas, NV, USA, 15–18 January 1995; pp. 83–88.
18. Gawthrop, P.J.; Palmer, D. A bicausal bond graph representation of operational amplifiers. *Proc. Inst. Mech. Eng. Part I J. Syst. Control* **2003**, *217*, 49–58. [\[CrossRef\]](#)
19. Samantaray, A.K.; Ghoshal, S.K. Bicausal bond graphs for supervision: From fault detection and isolation to fault accommodation. *J. Frankl. Inst.* **2008**, *345*, 1–28. [\[CrossRef\]](#)
20. Porter, B.; Bradshaw, A. Design of linear multivariable continuous-time tracking systems incorporating error-actuated controllers. *Int. J. Syst. Sci.* **1976**, *7*, 943–948. [\[CrossRef\]](#)
21. Gonzalez-A, G. Design of LTI tracking systems modelled by bond graphs. In Proceedings of the 2013 18th International Conference on Methods & Models in Automation & Robotics (MMAR), Miedzyzdroje, Poland, 26–29 August 2013.
22. Kahoul, R.; Azzouz, Y.; Ravelo, B.; Mazari, B. New Behavioral Modeling of EMI for DC Motors Applied to EMC Characterization. *IEEE Trans. Ind. Electron. (TIE)* **2013**, *60*, 5482–5496. [\[CrossRef\]](#)
23. Meng, D.; Xiao, Y.; Guo, Z.; Jolfaei, A.; Qin, L.; Lu, X.; Xiang, Q. A data-driven intelligent panning model for UAVs routing networks in mobile Internet of Things. *Comput. Commun.* **2021**, *179*, 231–241. [\[CrossRef\]](#)
24. Zhang, Q.; Yu, K.; Guo, Z.; Garg, S.; Rodrigues, J.J.P.C.; Hassan, M.M.; Guizani, M. Graph Neural Network-Driven Traffic Forecasting for the Connected Internet of Vehicles. *IEEE Trans. Netw. Sci. Eng.* **2021**. [\[CrossRef\]](#)
25. Olejnik, P.; Adamski, P.; Batory, D.; Awrejcewicz, J. Adaptive Tracking PID and FOPID Speed Control of an Elastically Attached Load Driven by a DC Motor at Almost Step Disturbance of Loading Torque and Parametric Excitation. *Appl. Sci.* **2021**, *11*, 679. [\[CrossRef\]](#)
26. Garcia-Sanchez, J.R.; Tavera-Mosqueda, S.; Silva-Ortigoza, R.; Guzman, V.M.H.; Sandoval-Gutierrez, J.; Marcelino-Aranda, M.; Marciano-Melchor, H.T.M. Robust Switched Tracking Control for Wheeled Mobile Robots Considering the Actuators and Drivers. *Sensors* **2018**, *18*, 4316. [\[CrossRef\]](#)
27. Gawthrop, P.; Smith, L. *Metamodeling*; Prentice-Hall: London, UK, 1996.
28. Sueur, C.; Dauphin-Tanguy, G. Bond graph approach for structural analysis of MIMO linear systems. *J. Frankl. Inst.* **1991**, *1*, 55–70. [\[CrossRef\]](#)
29. Dauphin-Tanguy, G.; Rahmani, A.; Sueur, C. Bond graph aided design of controlled systems. *Simul. Pract. Theory* **1999**, *7*, 493–513. [\[CrossRef\]](#)
30. Dauphin-Tanguy, G. *Les Bond Graphs*; Hermes: Paris, France, 2000.
31. Brown, F.T. *Engineering System Dynamics*; Dekker: New York, NY, USA, 1989.
32. Van Dijk, J.; Breedveld, P.C. Simulation of systems models containing zero-order causal paths—I. Classification of zero-order causal paths. *J. Frankl. Inst.* **1991**, *328*, 959–979. [\[CrossRef\]](#)